

Review

Exploration of porous metal–organic frameworks for gas separation and purification

Rui-Biao Lin^a, Shengchang Xiang^c, Huabin Xing^b, Wei Zhou^d, Banglin Chen^{a,*}^a Department of Chemistry, University of Texas at San Antonio, One UTSA Circle, San Antonio, TX 78249-0698, USA^b Key Laboratory of Biomass Chemical Engineering of Ministry of Education, College of Chemical and Biological Engineering, Zhejiang University, Hangzhou 310027, China^c College of Chemistry and Chemical Engineering, Fujian Provincial Key Laboratory of Polymer Materials, Fujian Normal University, 32 Shangsan Road, Fuzhou 350007, China^d NIST Center for Neutron Research, National Institute of Standards and Technology, Gaithersburg, MD 20899-6102, USA

ARTICLE INFO

Article history:

Received 15 August 2017

Received in revised form 22 September 2017

Accepted 29 September 2017

Available online 9 October 2017

Keywords:

Metal–organic frameworks

Gas separation/purification

Interpenetration

Metalloligand

Functionality

Pore engineering

ABSTRACT

As a new generation of porous materials, metal–organic frameworks (MOFs, also known as porous coordination polymers) have shown great promise for gas separation and purification because of their unique pore structures and surfaces for their differential recognition of small gas molecules. In this review article, we summarize our ongoing research endeavors to explore and discover microporous MOFs for gas separation and purification. We have developed several approaches to systematically tune the pores and to immobilize functional sites, including (1) the primitive cubic net of interpenetrated microporous MOFs from the self-assembly of the paddle-wheel clusters, $M_2(\text{CO}_2)_4$ ($M = \text{Cu}^{2+}, \text{Zn}^{2+}, \dots$), with two types of organic dicarboxylic acid and pillar bidentate linkers; (2) microporous mixed-metal–organic frameworks (M²MOFs) through the metallo-ligands, and (3) microporous MOFs with dual functionalities. Such efforts have enabled us to make some breakthroughs on microporous MOFs for gas separation and purification, as demonstrated in the gas chromatographic separation of hexane isomers, kinetic D_2/H_2 separation, acetylene/ethylene separation, carbon dioxide capture, $\text{C}_2\text{H}_2/\text{CO}_2$ and $\text{C}_3\text{H}_4/\text{C}_3\text{H}_6$ separation. Our group is one of the first groups who have envisioned the practical promise of microporous MOFs for the industrial gas separation and examined their separation capacities and efficiency using the fixed-bed adsorption and/or breakthrough experiments. Some of the very important and representative examples of these microporous MOFs for diverse gas separation and purification are highlighted in this review.

© 2017 Elsevier B.V. All rights reserved.

Contents

1. Introduction	88
2. Pore engineering of MOFs for gas separations and purification	89
2.1. Separation of alkane isomers	89
2.2. Kinetic D_2/H_2 separation	90
2.3. Separations of $\text{C}_2\text{H}_2/\text{C}_2\text{H}_4$	91
2.4. Sulfur dioxide capture	95
2.5. Carbon dioxide capture	96
2.6. Separations of $\text{C}_2\text{H}_2/\text{CO}_2$	98
2.7. Separations of $\text{C}_3\text{H}_4/\text{C}_3\text{H}_6$	100
3. Conclusion and outlook	101

Abbreviations: RON, Research Octane Number; nHEX, *n*-hexane; 2MP, 2-methylpentane; 3MP, 3-methylpentane; 22DMB, 2,2-dimethylbutane; 23DMB, 2,3-dimethylbutane; H_2bdc , 1,4-benzenedicarboxylic acid; bpy, 4,4'-bipyridine; dabco, 1,4-diazabicyclo[2,2,2]octane; PyenH₂, 5-methyl-4-oxo-1,4-dihydro-pyridine-3-carbaldehyde; H_2cdc , 1,4-cyclohexanedicarboxylate acid; H_2atbdc , 5-(5-amino-1H-tetrazol-1-yl)-1,3-benzenedicarboxylic acid; BET, Brunauer-Emmett-Teller; DFT-D, dispersion-corrected density-functional theory; Hcit, citric acid; H_4dobdc , 2,5-dioxido-1,4-benzenedicarboxylic acid; dps, 4,4'-dipyridylsulfide.

* Corresponding author.

E-mail address: banglin.chen@utsa.edu (B. Chen).

Acknowledgement	101
Appendix A. Supplementary data	101
References	101

1. Introduction

Separation and purification processes are critically important for modern chemical industry as to isolate pure or purer components from chemical mixtures, which accounts for about half of industrial energy consumption. Gas separation, such as hydrocarbon separation and natural gas processing, is widely involved in the production of bulk chemical products for manufacturing fuels, plastics and polymers [1–3]. Traditional gas separation technologies based on distillation or liquid absorbent are highly energy-intensive and capital-intensive. For distillation, repeated evaporating-condensing cycle of the mixture under harsh conditions are required, while the regeneration of liquid absorbent during a complete separation cycle involves heating and cooling of massive solvent medium to release adsorbed gas. In contrast, non thermal alternatives to distillation, such as using porous solid for adsorptive separation based on the molecular properties (chemical affinity or molecular size) of the separated components, have been proposed as more energy efficient technologies [4–8]. For example, membrane-based separation technologies only consume about 10% energy of that for distillation [9]. However, the separation efficiency of these developing technologies relies on the internal porosity and surface properties of solid adsorbents due to their key role in gas sorption.

Compared with classical adsorbents such as zeolite silicates and carbon-based materials, metal–organic frameworks (MOFs) and/or porous coordination polymers are novel customizable porous materials affording precise tuning and functionalization of the pore structure. MOFs can be self-assembled straightforwardly through the coordination of suitable organic linkers to metal ions/clusters. Unlike porous zeolite silicates mainly constructed by SiO₄ tetrahedra linking through O²⁻/OH⁻, the infinite combinations of various metal ions and organic ligands for constructing porous MOFs have provided a vast variety of new porous materials that show diverse structures and porosity. MOFs are unparalleled in terms of their uniform pore structures, high crystallinity, high porosity, diversified/designable structures and tunable pore sizes [10,11]. Importantly, the pores/channels sizes within MOFs can be systematically tuned by using organic ligands of different lengths to coordinate respectively with metal ions [12–14]. For example, rational design can give rise to high porosity with surface area up to 7000 m² g⁻¹ and pore sizes ranging from 3 to 100 Å [10]. Furthermore, by virtue of substituted linkers and uncoordinated sites, many types of functional sites (Lewis basic or acidic sites, polar amino or hydroxyl groups, open metal sites etc.) can be readily immobilized onto the pore surfaces for recognition of specific molecules. Such unique features have enabled MOFs to exhibit great potentials in applications of gas storage [15–20], gas separations [21–26], molecular recognition [27–30], heterogeneous catalysis [31–36], chemical sensing [37–41] and drug delivery and so on [42–46].

Research on MOFs is certainly one of the most active research fields among chemistry and materials science community over the past two decades [10,47–52]. The early endeavours in the community mainly focused on porous MOFs for related applications to use their porosity such as gas storage, separation, and heterogeneous catalysis. The potential to utilize porous structures of coordination polymers for gas adsorption was initially proposed in 1997 [53,54]. The realization of the first few porous MOFs with

permanent porosity established by gas adsorption studies significantly facilitated the development of these novel adsorbents for gas storage and separation [55,56]. After few explorations at the early stage, an explosive increasing of the research on porous MOFs for gas storage and separation has been witnessed [10,48,50,57,58]. For selective gas separation, most of the early research during this period was conducted based on single-component adsorption/desorption isotherm measurements of pure gases. The accumulation of sorption data from numerous MOFs made adsorbent screening a reality, which also illustrated an encouraging potential for separation and purification of gas or vapor mixtures. However, actual separation of gas mixtures using MOFs was scarcely realized until gas chromatography as a new evaluating method was introduced into this field at about 2005 [59]. Later in 2007, experimental fixed-bed breakthrough also for the first time was applied on the evaluation of separation performance of MOF materials [60]. Based on these technologies, MOFs have demonstrated real separation of gas mixtures originated from their intrinsic porous properties. Therefore, breakthrough experiment became a powerful tool for separation performance evaluation of MOFs, which can mimic the industrial process that cannot be revealed by simple static single-component gas sorption study. Since then, quite a number of important and challenging separations, such as carbon dioxide capture and separation from methane or nitrogen, light hydrocarbons separation, isomers separation, noble gases separation etc., have been achieved by making use of the unique MOFs as adsorbent materials [3,8].

Based on the size/shape of the adsorbent's pore and/or the binding affinity from adsorption sites, the adsorptive separation of gas mixtures can be realized by differentiating the adsorbate molecular sizes, shapes, polarities, polarizabilities, coordination abilities, conformations, and so on [3,8,61–62]. Therefore, separation based on different mechanisms can be roughly classified as thermodynamic separation, kinetic separation, molecular sieving and conformational separation. Thermodynamic separation usually happens in relatively large pore structure and can be attributed to different binding affinities to adsorbate molecules, which are mainly related to their various host–guest interactions. Such binding strength is usually reflected by isosteric adsorption heat at zero coverage, which can be enhanced by introducing strong binding sites. Kinetic separation originates from the diffusivity difference of adsorbed molecules when diffusing along the pore channel. In this type of separation, gas molecules with relatively high mobility can occupy the pore spaces firstly, resulting in separation before the adsorption equilibrium of other components. Such nonequilibrium gas separation can be realized in transient fixed bed separations, although it might not be reflected by the sorption isotherms of different gas components. Molecular sieving, based on the inaccessibility of pore spaces to certain gas components during a sufficiently long period of time (e.g., the equilibrium time set for gas sorption measurements), is often considered as the ultimate separation approach due to their infinite selectivity for specific gas molecules. In molecular sieving, MOF with suitable pore size/shape allows accommodating of relatively small molecules while excluding the larger ones. For closely related organic molecules (with very similar physical properties, Fig. 1), completely separating their mixtures is highly challenging, thus only very few MOFs can realize such exclusive separation. Conformational separation usually happens in relatively large pore structure when the host–guest

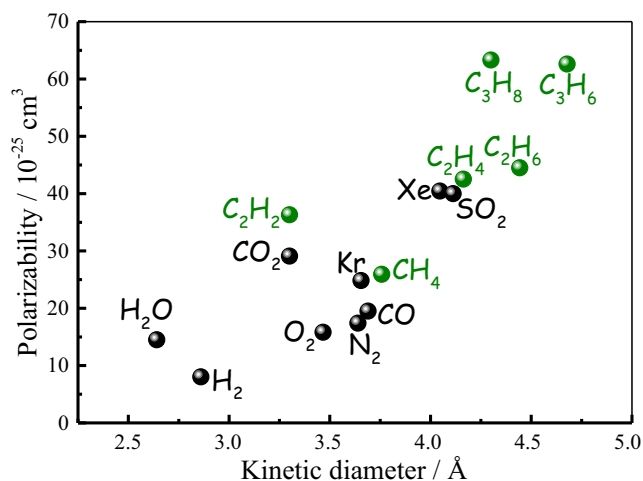


Fig. 1. Important physical parameters of selected gas adsorbates. Light hydrocarbons are highlighted in green.

interactions between adsorbates and adsorbents are almost the same, and only packing efficiency can serve as the initiative driving force. Overall, for separating a given mixture, both parameters of MOFs and adsorbates should be taken into account. In general, adsorbents of small pore size can show high selectivity but low uptake capacity, while large pore size can afford high capacity but low selectivity. For highly efficient separation, MOFs should exhibit well-balanced adsorption capacity and selectivity. Therefore, precise structure controlling over pore surface and pore size is highly demanded.

Certainly, besides excellent separation performance, ideal adsorbents should take other important factors into account, including physical and chemical stability, recyclability, regeneration, cost, scale-up of production etc. Among these factors, the water/moisture stability is crucial for the application of MOF adsorbents considering the operation conditions involved in realistic environment [63]. Although the coordination bonds might be not as strong as the covalent bonds, there are more and more water-stable MOFs composed of ligands of high pK_a values and high oxidation state metal ions for strong coordination ability. There are also some approaches to enhance the stability of sensitive MOFs, involving functionalization MOFs with hydrophobic moieties, surface modification via postsynthesis, and framework interpenetration. As the exploration of MOF adsorbents goes in deep, closer collaboration with chemical engineering scientists and industrial partners will be enforced for their practical applications.

Fast development and significant progress of porous MOFs have been witnessed over the past two decades. As clearly demonstrated, pore engineering is powerful to control the pore structure and functionality, which dramatically promote the development of MOFs for differential molecule recognition. We have been able to engineer the pores of MOFs through the tuning of their pore sizes/channels, surface areas and functional sites to target novel MOF materials for specific gas separations [64,65]. This review focuses on our ongoing research endeavours during the exploration and discovery of microporous MOFs for gas separation and purification. Specifically, three approaches have been developed to systematically tune the pores and to immobilize functional sites, including (1) interpenetration of microporous MOFs with the primitive cubic net from the self-assembly of the paddle-wheel clusters, $M_2(\text{CO}_2)_4$ ($M = \text{Cu}^{2+}$, Zn^{2+} and other transition metal ions), linking by two types of organic dicarboxylic acid and pillar bidentate linkers; (2) construction of microporous mixed-metal-organic

frameworks (M'MOFs) through the metalloligands to immobilize open metal sites, and (3) microporous MOFs with dual functionalities showing suitable pore/cage spaces and functional groups on the pore/cage surfaces. Our continuous efforts on pore and function engineering have enabled us to make some breakthroughs on microporous MOFs for gas separation and purification, as demonstrated in the gas chromatographic separation of hexane isomers, kinetic separation of hydrogen isotope, acetylene/ethylene separation, carbon dioxide capture, acetylene/carbon dioxide and propylene/propyne separation. Our group is one of the first groups who have envisioned the practical promise of microporous MOFs for the industrial gas separation and realized to evaluate their separation capacities and efficiency using the fixed-bed adsorption and/or breakthrough experiments. Some of the very important and representative examples of these microporous MOFs for diverse gas separation and purification are highlighted in this review.

2. Pore engineering of MOFs for gas separations and purification

During our exploration of microporous MOFs for gas separation, pore engineering through the above-mentioned functionalization strategies is strongly confirmed as a powerful tool for efficient separation of different gases. Extending from preliminary exploration [66–71], controlling over the pore sizes and functional sites collaboratively afforded differential recognitions and accommodations of gas molecules [72–84].

2.1. Separation of alkane isomers

The separation of linear alkanes from their branched isomers can boost octane ratings in gasoline, which is a very important process in the petroleum industry. This is because, comparing with linear alkanes, the branched isomers show higher Research Octane Number (RON) values that are dependent on the branching degree [85]. For example, the RON values of hexane isomers are 30 for *n*-hexane (nHEX), 74 for 2-methylpentane (2MP), 75 for 3-methylpentane (3MP), 94 for 2,2-dimethylbutane (22DMB) and 105 for 2,3-dimethylbutane (23DMB). To achieve higher octane number fuels, the mixture is processed by zeolites to sieve nHEX followed by the distillation of the monobranched isomers [86]. Improved hexane-separation process to efficiently isolate valuable dibranched hexanes is crucially necessary to meet cost-efficient demand. Hexane isomers are composed of carbon atoms that are linked via carbon–carbon single bonds and further saturated by hydrogen atoms. Due to the negligible dipole moments of hexane isomers, their interactions with other chemical species are mainly weak interactions such as van der Waals interactions, which make it greatly challenging to direct specific interactions for their selective recognition. Thus, the control of pore size is very important for alkanes (hexane isomers) separation, as it can be an effective approach to differentiate the components based on their sizes difference. In contrast, for important C8 alkylaromatic compounds such as xylene isomers [87–89], their relatively larger polarizabilities allow the separation of their mixtures to achieve mainly through different host–guest interactions rather than only depending on the pore size of adsorbents. In fact, few MOFs can show selective accommodation of specific alkanes [90].

The first example of using microporous MOF to separate alkane isomers was reported by Chen et al. in 2005 [59]. The linear and branched isomers of pentane and hexane has been successfully separated in a gas-chromatographic (GC) column of a double interpenetrated MOF, $[\text{Zn}_2(\text{bdc})_2(\text{bpy})]$ (MOF-508, $\text{H}_2\text{bdc} = 1,4$ -benzene dicarboxylic acid; $\text{bpy} = 4,4'$ -bipyridine), which is composed of 6-connected paddle-wheel zinc clusters bridged by bdc^{2-} and

bpy linkers to form three dimensional framework with **pcu** topology. The as-synthesized MOF-508a contains one-dimensional channels of about 4.0 Å in diameter (Fig. 2), which are slightly larger than the size of methane (kinetic diameter: 3.8 Å), being accessible for linear alkanes but excluding their branched parts. Such microporous MOF column shows great potential in the efficient GC separation of natural gas and alkane mixtures. As evident by GC measurements, the alkanes isomers can be well separated from their mixtures by the column of MOF-508, generating a retention time hierarchy of linear > monobranched > dibranched isomer. Thus, for hexane isomers, pure 22DMB eluted firstly from the column, followed by 2MP, while their linear isomer nHEX shows the longest retention time. Similarly, branched 2-methylbutane can be separated from its linear isomer *n*-pentane. The selective GC separation of alkanes on the MOF-508 column was attributed to their different van der Waals interactions with the inner pore surface of MOF-508. The shorter linear part of alkane would result in a weaker van der Waals interaction and elutes faster from its isomers. Thus, the retention time of an alkane mainly depends on the length of its linear part, affording efficient separation of alkanes.

The micropores in similar MOFs can be rationally tuned by controlling their interpenetration number. After the above pioneering work, the separation of hexane isomers was further realized on microporous MOF through experimental fixed-bed breakthrough for the first time by Chen et al. [60]. The non-interpenetrated microporous MOF [Zn₂(bdc)₂(dabco)] (dabco = 1,4-diazabicyclo[2,2,2]octane) is three dimensional framework with **pcu** topology composed of paddle-wheel zinc cluster nodes and bdc²⁻/dabco linkers, showing good kinetic separation of hexane isomers by fixed-bed adsorption. Different from the above-mentioned interpenetrated MOF-508, there are two types of intersecting channels of about 7.5 Å × 7.5 Å and 3.8 Å × 4.7 Å along different directions (Fig. 3), respectively. Because the size of the large channels (7.5 Å) is larger than the kinetic diameters of nHEX (4.3 Å), 3MP (5.0 Å), and 22DMB (6.2 Å), it is expected that all the isomers have

the access to the large channels while nHEX shows stronger van der Waals interactions with the framework attributed to its linear shape and smaller size. For the narrow channels, it is only accessible to linear nHEX but blocks the branched isomers, affording this MOF to kinetically separate mixture of hexane isomers. Then, the potential of this MOF for hexane isomers separations were checked first by single-component breakthrough experiments, resulting in a breakthrough time hierarchy of nHEX > 3MP > 22DMB. Further binary and ternary breakthrough experiments using this MOF confirmed its capability to isolate the monobranched 3MP and dibranched 22DMB hexane isomers from linear nHEX isomer.

Notably, based on rationally tuned micropores, the aforementioned endeavours realized porous MOFs for the challenging separation of alkane isomers, which has initiated extensive research of exploration on MOFs for this very important industrial application. Those followed improved results further demonstrated the applicable of MOFs for hydrocarbons separation [91,92]. Importantly, using gas chromatography/fixed-bed adsorber as powerful tool to evaluate mixture separation has significantly facilitated the development of alkanes separation technology.

2.2. Kinetic D₂/H₂ separation

Deuterium is a stable isotope of hydrogen that has a number of commercial and scientific applications. The isotopic separation is necessary for deuterium production considering its low abundance (0.0156% of all the naturally occurring hydrogen) [94]. Compared with traditional techniques like chemical exchange method (Girdler sulfide process) and cryogenic distillation (at 24 K), gaseous isotope separation by cryogenic gas adsorption in porous materials was proposed as an energy-efficient alternative. However, conventional size exclusion mechanism (molecular sieves) cannot be applied on the separation of isotopic H₂/D₂ because of their nearly identical sizes, shape, and thermodynamic properties. In fact, it is proposed that kinetic quantum molecular sieving mechanism based on quantum effect involved in adsorption/desorption of H₂

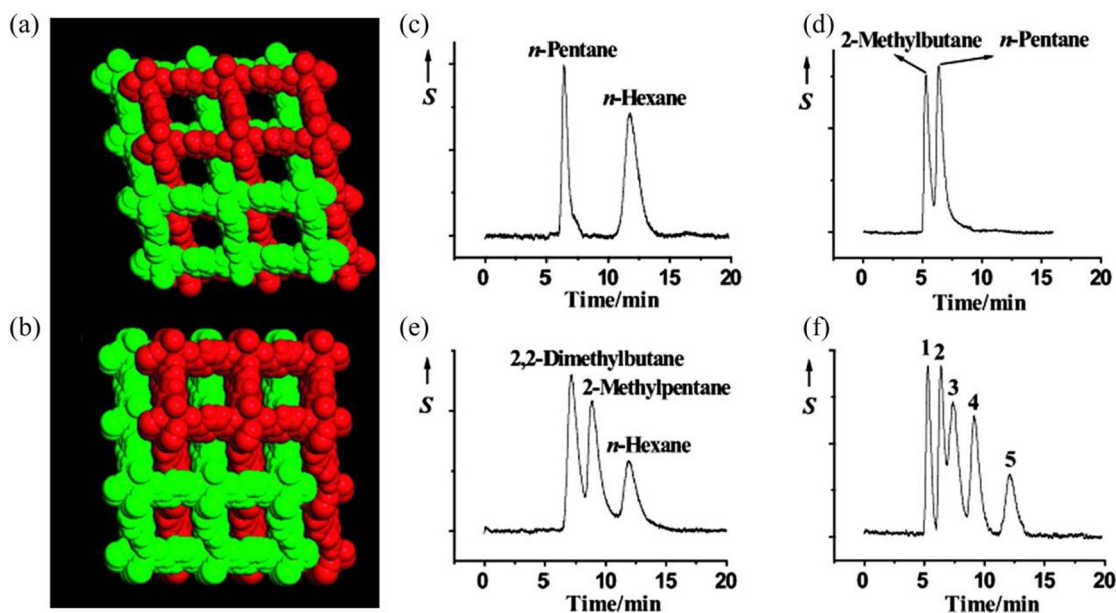


Fig. 2. Space-filling packing structures diagram of (a) the open phase MOF-508a, which contains 1D channels of 4.0 Å × 4.0 Å, and (b) the dense phase MOF-508b, viewed along the rectangular diagonal of the paddle-wheel clusters. The disordered guest molecules in MOF-508a are omitted for clarity. The two interpenetrating frameworks are shown in red and green. (c–f) Chromatograms of alkane mixtures separated on a MOF-508 column: (c) separation of *n*-pentane and *n*-hexane, (d) separation of 2-methylbutane and *n*-pentane, (e) separation of 2,2-dimethylbutane, 2-methylpentane, and *n*-hexane, and (f) separation of an alkane mixture containing 2-methylbutane (1), *n*-pentane (2), 2,2-dimethylbutane (3), 2-methylpentane (4), and *n*-hexane (5). S-thermal conductivity detector response. Reprinted with permission from Ref. [59]. Copyright 2006 Wiley-VCH.

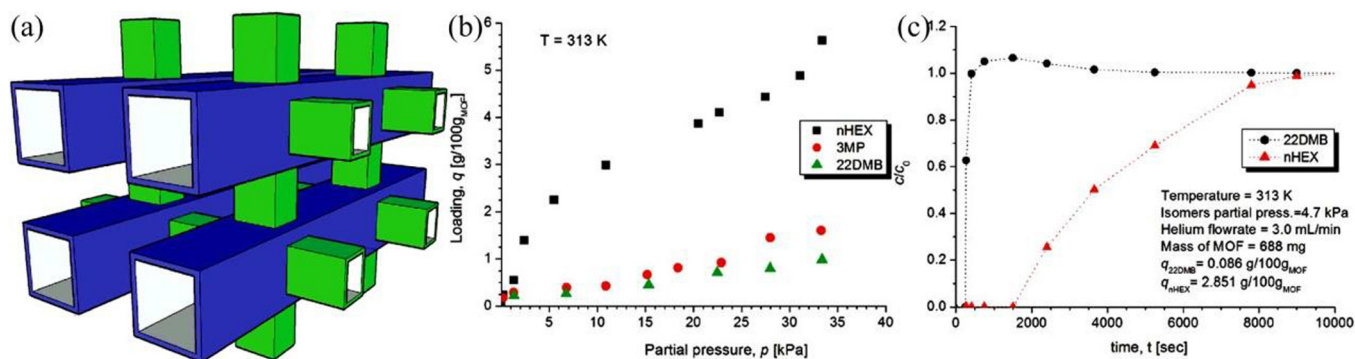


Fig. 3. (a) Perspective illustration of 3D intersecting channels in Zn(BDC)(Dabco)_{0.5} of $7.5 \text{ \AA} \times 7.5 \text{ \AA}$ and $3.8 \text{ \AA} \times 4.7 \text{ \AA}$ along different directions, shown in blue and green, respectively. (b) Pure-component adsorption isotherms of 22DMB (green), 3MP (red), and nHEX (black) at $T = 313$ K. (c) Binary breakthrough curve for an equimolar mixture of 22DMB/nHEX at $T = 313$ K. Points are experimental data, and dotted lines are for clarity. Reprinted with permission from Ref. [60]. Copyright 2007 American Chemical Society.

and D_2 within confined narrow pore system. Such kinetic separation is achieved through different diffusion barriers from the difference in the zero-point energy of the adsorbed H_2/D_2 isotopes. Kinetic quantum molecular sieving may be observed for H_2/D_2 adsorption when the difference between the molecular diameter and the pore diameter of adsorbents becomes comparable to the de Broglie wavelength, which usually happens in pore structure of about 0.6 nm. For example, Kaneko et al. reported that [Cu(bpy)₂(CF₃SO₃)₂] with two different pores of 8.7 and 2.0 Å can separate H_2/D_2 mixture at 77 K with a selectivity of 1.2 [95]. Also, open metal sites in MOFs can enlarge the binding difference of H_2/D_2 with the framework, thus realize their separation. For example, FitzGerald et al. reported that the D_2 adsorption heat in Ni-MOF-74 is larger than that for H_2 with a difference of 1.4 kJ mol^{-1} , resulting a zero-pressure selectivity of 5 at 77 K [96]. Simultaneously, incorporating open metal centers into ultramicropore MOFs for binding hydrogen molecules under the confinement of pore space not only can enhance the hydrogen binding affinity but also maximize the quantum effects, affording higher performance of kinetic H_2/D_2 separation. As a rational strategy that can systematically immobilize different open metal sites within porous MOFs, metalloligand approach is very promising on this endeavor. The first experimental results for H_2/D_2 separation using MOFs were published in 2008 [93]. We developed a microporous mixed-metal-organic framework (M'MOF) [Zn₃(bdc)₃(CuPyen)] (M'MOF-1, PyenH₂ = 5-methyl-4-oxo-1,4-dihydro-pyridine-3-carbaldehyde) with enhanced affinity for hydrogen molecules, which successfully separated D_2 from H_2 through kinetic quantum molecular sieving. M'MOF-1 is composed of trinuclear Zn₃(RCOO)₆ clusters bridged by bdc²⁻ and preconstructed metalloligand Cu(Pyen) to form three dimensional framework with two types of micropores ($\leq 5.6 \text{ \AA}$, Fig. 4). The immobilized Cu centers with two open sites on the pore surface are accessible for gas molecules after activation. Adsorption measurements for H_2 and D_2 revealed comparable molar D_2/H_2 ratios (nD_2/nH_2) of 1.09–1.11 attributed to quantum effect. The isosteric enthalpies of adsorption ($Q_{st,n=0}$) at zero surface coverage were calculated to be $12.29(53)$ and $12.44(50) \text{ kJ mol}^{-1}$ for H_2 and D_2 , respectively. Adsorption kinetics analyses for the diffusion of H_2 and D_2 during adsorption in M'MOF-1 revealed that the heavier D_2 were faster than H_2 , showing average ratios of rate constants k_{D_2}/k_{H_2} of 1.62 and 1.38 for two components (k_1 and k_2), respectively, corresponding to diffusion along two types of pores. The D_2 kinetic barriers (activation energy) related to its zero-point energy were determined to be 12.52 and 8.04 kJ mol^{-1} for both components, which are slightly lower than the corresponding values for H_2 kinetics for both components. Such difference of adsorption kinetics was attributed to quantum effects that the

higher effective collision cross section of H_2 related to its higher zero point energy can result in a higher barrier for diffusion along the pores as compared to D_2 , which might be utilized for the kinetic sieving H_2/D_2 separation. This is the first experimental observation of porous MOF materials for kinetic isotope quantum molecular sieving.

Notably, by virtue of metallo-ligand approach, the above endeavour firstly realized porous MOFs for the challenging kinetic sieving H_2/D_2 separation. After this pioneering work, extensive research interests have been attracted to explore MOFs on kinetic isotope quantum molecular sieving [62,97], affording further improved performance for this very important application.

2.3. Separations of C_2H_2/C_2H_4

Ethylene (C_2H_4 , the most produced organic compound in the world, over 150 million tons/year in 2016) is essential raw chemical widely used in the manufacture of many polymer products and useful chemicals. Ethylene is produced in the petrochemical industry by steam cracking, accompanied by some other byproducts and/or impurities. Among them, acetylene is one important byproduct/impurity of approximately 1% concentration, because it can seriously affect the polymerization of ethylene by poisoning the catalyst during the production of polyethylene, a most important and widely used plastic. Also, acetylene is explosive above 200 kPa (29 psi), and can form solid metal acetylides that would block the cracked gas stream, resulting in huge safety risk. Therefore, during the ethylene production, acetylene must be reduced to an acceptable level. To meet the concentration limit of below 40 ppm (parts per million), cryogenic distillation or partial hydrogenation are applied to remove or transform acetylene, which is energy intensive. In contrast, adsorptive separation using MOFs for this challenging acetylene removal provide a more efficient way, avoiding the use of noble metals and solvents, which has attracted great interest. Also, adsorptive acetylene capture can produce pure acetylene gas to better utilize and meet the industrial need [98]. In fact, the adsorptive separation performance of MOFs for the acetylene/ethylene mixture has been extensively examined, but only a few of them show some promise. This is because acetylene and ethylene show similar molecular sizes, polarizabilities, dipole moments and other physical/chemical properties.

Xiang et al. reported the first example of microporous MOFs for this challenging acetylene/ethylene separation in 2011 [99]. Isostructural mixed-metal-organic frameworks (M'MOFs) have been developed from metalloligand Cu(SalPycy) by systematically tuning their micropores for optimized C_2H_2/C_2H_4 selectivities. Two M'MOFs Zn₃(bdc)₃[Cu(SalPycy)] (M'MOF-2) and Zn₃(cdc)₃[Cu

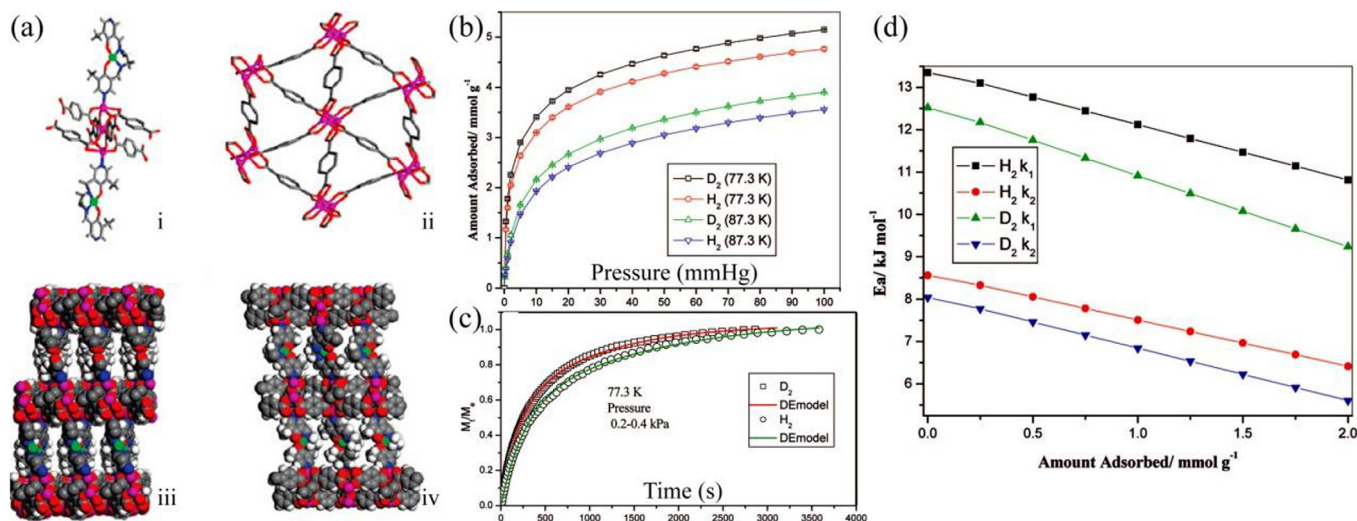


Fig. 4. (a) X-ray crystal structure of M'MOF-1 [$\text{Zn}_3(\text{bdc})_3\text{Cu}(\text{Pyen})$] showing (i) one trinuclear $\text{Zn}_3(\text{COO})_6$ secondary building unit, (ii) one 36 tessellated $\text{Zn}_3(\text{bdc})_3$ 2-D sheet that is pillared by the $\text{Cu}(\text{Pyen})$ to form a 3-D microporous M'MOF-1 having (iii) curved pores of about $5.6 \text{ \AA} \times 12.0 \text{ \AA}$ and (iv) irregular ultramicropores along different directions. Color scheme: Zn (magenta), Cu (green), O (red), N (blue), C (gray), H (white). (b) Isotherms for H_2 and D_2 adsorption on M'MOF-1 at 77.3 and 87.3 K. (c) Comparison of H_2 and D_2 kinetic profiles and the corresponding fitting for DE kinetic model for adsorption on M'MOF-1 at 77.3 K (0.2–0.4 kPa). (d) The variation of activation energy (E_a , kJ mol^{-1}) with amount adsorbed (mmol/g) for H_2 and D_2 adsorption on M'MOF-1. Reprinted with permission from Ref. [93]. Copyright 2008 American Chemical Society.

(SalPycy)] (M'MOF-3, $\text{H}_2\text{cdc} = 1,4\text{-cyclohexanedicarboxylate acid}$) (Fig. 1) were readily assembled by solvothermal reactions of pre-designed metalloligand $\text{Cu}(\text{SalPyCy})$ with $\text{Zn}(\text{NO}_3)_2 \cdot 6\text{H}_2\text{O}$ and $\text{H}_2\text{bdc}/\text{H}_2\text{cdc}$ (Fig. 5), exhibiting chiral pore cavities with immobilization of open Cu centers. M'MOF-2 and M'MOF-3 are isostructural three dimensional frameworks, in which trinuclear $\text{Zn}_3(\text{RCOO})_6$ clusters are connected by bdc^{2-} or cdc^{2-} ligands to form two dimensional $\text{Zn}_3(\text{bdc})_3$ or $\text{Zn}_3(\text{cdc})_3$ layers that are further pillared by the chiral metalloligand $\text{Cu}(\text{SalPyCy})$. Due to the more flexible cdc^{2-} ligand, activated M'MOF-3a has smaller pores as compared to M'MOF-2a, which is confirmed by adsorption isotherms of CO_2 at 195 K. Thus, at 195 K, M'MOF-3a exhibited a significantly higher $\text{C}_2\text{H}_2/\text{C}_2\text{H}_4$ selectivity of 25.5, while M'MOF-2a

can adsorb both C_2H_2 and C_2H_4 resulting in a low selectivity of 1.6. The higher selectivity of M'MOF-3a was attributed to enhanced sieving effects in M'MOF-3a. Compared with the molecular size of C_2H_4 (kinetic diameters: 4.2 \AA), the smaller C_2H_2 (3.3 \AA) allowed it to fulfill more efficient filling in the micropores of M'MOF-3a. In contrast, C_2H_4 molecules are basically blocked or the kinetics is very slow. Remarkably, the $\text{C}_2\text{H}_2/\text{C}_2\text{H}_4$ selectivity of M'MOF-3a at 295 K was calculated to be 5.2, making this material a practically promising adsorbent for this important separation. Overall, the subtle tuning of the micropores in metalloligand-based MOFs resulted in significantly enhanced $\text{C}_2\text{H}_2/\text{C}_2\text{H}_4$ separation.

The $\text{C}_2\text{H}_2/\text{C}_2\text{H}_4$ selectivities of these M'MOFs can be further optimized after systematically tuning their micropores by combining

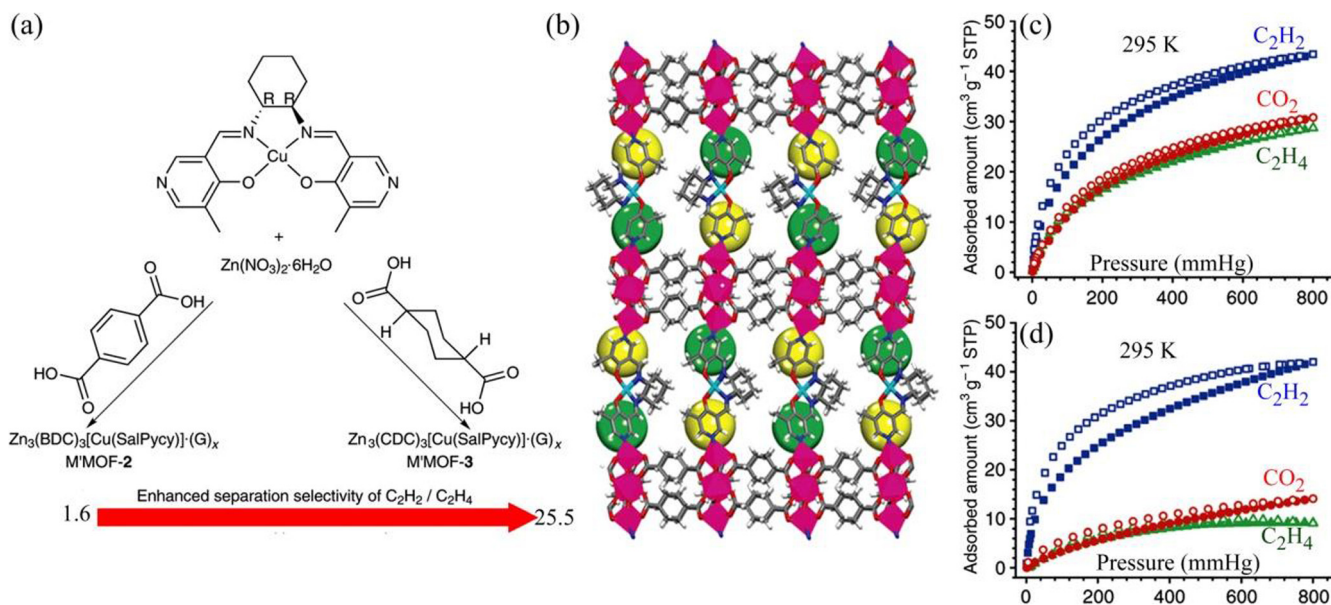


Fig. 5. (a) Schematic diagram for the synthesis of M'MOF-2 and M'MOF-3. (b) The three-dimensional pillared framework with chiral pore cavities for M'MOF-3. (c-d) Adsorption isotherms of C_2H_2 (blue square), CO_2 (red dot) and C_2H_4 (green triangle) on (c) M'MOF-2a and (d) M'MOF-3a at 295 K. Reproduced with permission from Ref. [99]. Copyright 2011 Nature Publishing Group.

different metalloligands and organic ligands, as revealed by series isostructural M'MOFs [27]. These activated M'MOFs are promising for effective removal of trace C_2H_2 from 1/99 C_2H_2/C_2H_4 mixture at room temperature. These M'MOFs can reduce the C_2H_2 concentration to below 40 ppm to meet the polymerization requirement, resulting in high purity ethylene. The potential application of these M'MOFs for the fixed-bed adsorptive separation of C_2H_2/C_2H_4 at ambient conditions has been further confirmed by transient breakthrough simulations. Among different M'MOFs, M'MOF-4a showed the best C_2H_2/C_2H_4 separation performance. Obviously, the sieving effects from the ultra-micro pores of these M'MOFs resulted in high C_2H_2/C_2H_4 selectivities. However, the small pore volumes would simultaneously limit their acetylene adsorption capacity, which definitely affects their actual performance for C_2H_2/C_2H_4 separation. Further development was extended to the evaluation of M-MOF-74 series with open metal sites for C_2H_2/C_2H_4 separation in 2012 [100]. Notably, Fe-MOF-74 reported by Long et al. can exhibit remarkable C_2H_4/C_2H_6 and C_3H_6/C_3H_8 separation with selectivities of 13–18 and 13–15, which is higher than classical adsorbents such as zeolite NaX and other MOFs [22]. Such separation is attributed to the much stronger interactions of ethylene and propylene with the metal sites as confirmed by neutron powder diffraction experiments. Indeed, by virtue of high densities of open metal sites, these M-MOF-74 materials indeed showed high uptake capacity and strong binding affinity for unsaturated hydrocarbons including acetylene. However, the C_2H_2/C_2H_4 selectivities of M-MOF-74 are quite low because the open metal sites can also bind strongly with ethylene.

Ideal porous materials for C_2H_2/C_2H_4 separation should exhibit high C_2H_2/C_2H_4 selectivity and optimal C_2H_2 adsorption capacity at ambient conditions. Dual-functionalized MOFs with suitable pore/aperture size and accessible strong binding sites can make it a reality [102]. After our extensive research endeavours on microporous MOFs for C_2H_2/C_2H_4 separation [103–107], we

recently realized a unique dual-functionalized MOF [Cu(atbdc)] (UTSA-100, $H_2atbdc = 5-(5\text{-amino-1H-tetrazol-1-yl})\text{-1,3-benzene dicarboxylic acid}$) for efficient removal of acetylene from 1/99 C_2H_2/C_2H_4 mixture [101]. This MOF is composed of 6-connected paddle-wheel copper clusters bridged by 3-connected atbdc²⁻ linkers to form three dimensional framework with **apo** topology. UTSA-100a contains one-dimensional channels of about 4.3 Å and small cavities of 4.0 Å with apertures of 3.3 Å (Fig. 6), exhibiting considerable Brunauer-Emmett-Teller (BET) surface area of 970 $m^2 g^{-1}$. Thanks to suitable pore sizes and immobilized $-NH_2$ groups as binding sites, UTSA-100a took up considerable C_2H_2 of 95.6 $cm^3 g^{-1}$ but much lower C_2H_4 of 37.2 $cm^3 g^{-1}$ at ambient conditions, resulting in high C_2H_2/C_2H_4 selectivity (10.7) for 1/99 C_2H_2/C_2H_4 mixture. The combination of high adsorption selectivity and high uptake capacity at ambient conditions allows UTSA-100a to remove trace C_2H_2 more efficiently (showing higher C_2H_2 adsorption capacity from 1/99 C_2H_2/C_2H_4 mixture), compared with the above mentioned M'MOFs, M-MOF-74 series and NOTT-300. The superior performance of UTSA-100a in trace acetylene removal was confirmed by simulated and experimental breakthrough studies. Detailed pore structure analysis and first-principles DFT-D (dispersion-corrected density-functional theory) calculations revealed that suitable pore size and binding sites play roles for highly efficient C_2H_2/C_2H_4 separation of UTSA-100a.

As demonstrated above, those MOF materials already have improved separation performance as compared to classical materials, but they still suffer from the trade-off of adsorption capacity versus selectivity for C_2H_2/C_2H_4 separation. This trade-off problem can be overcome through pore chemistry and size control. Very recently, Xing and Chen et al. reported a series of SiF_6^{2-} -pillared MOF materials (SIFSIX) with tunable pore sizes, providing a unique platform for optimizing host-guest and/or guest-guest interactions, which exhibit exceptional C_2H_2 capture performance for C_2H_2/C_2H_4 mixtures [108]. In these pillar-layered SIFSIX materials,

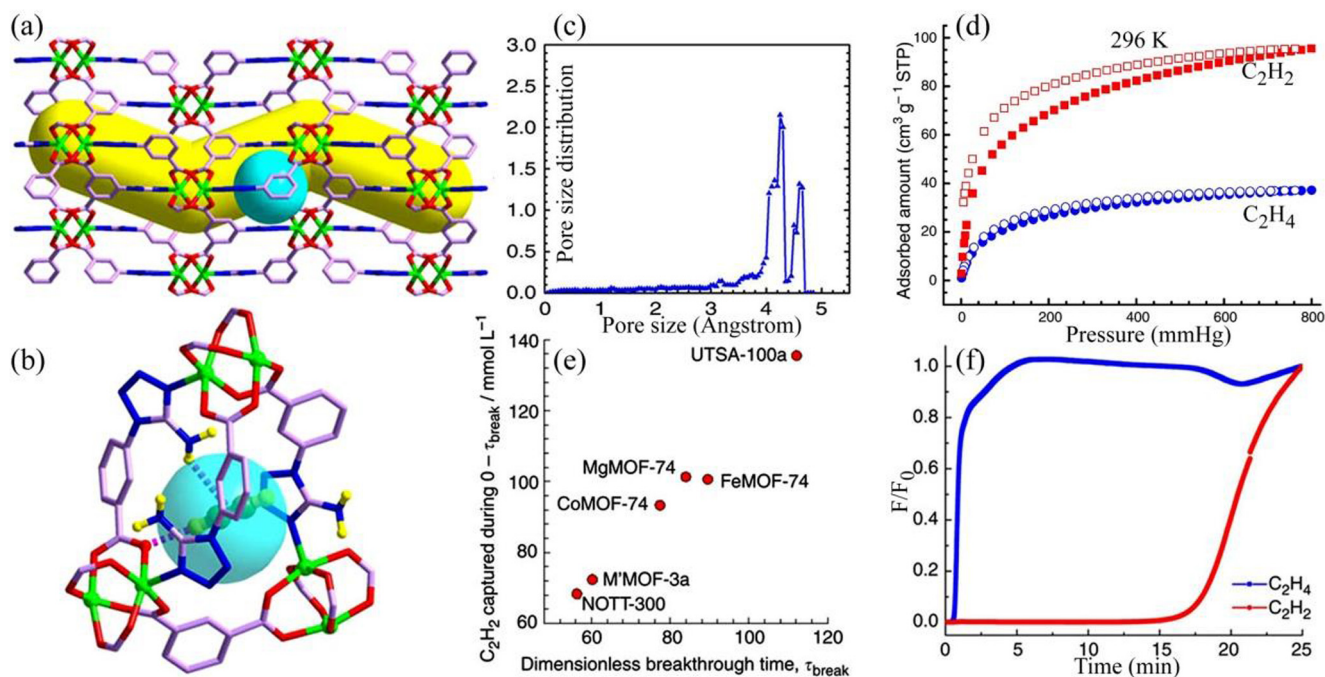


Fig. 6. (a) Pore structure showing the zigzag channels along the *c* axis and the cage with the diameter of about 4.0 Å in the pore wall with the window openings of 3.3 Å. (b) The acetylene locates right at the small cage connecting two adjacent channel pores. (multiple-point interactions of the acetylene molecule with framework: $d[O(-CO_2) \cdots H(C_2H_2)] = 2.252 \text{ \AA}$, $d[H(-NH_2) \cdots (C_2H_2)] = 2.856 \text{ \AA}$). (c) Pore size distribution (PSD) of UTSA-100a. (d) Acetylene (red) and ethylene (blue) sorption at 296 K. (e) Diagram of C_2H_2 captured per liter of adsorbent (<40 ppm of C_2H_2 in outlet gas), during the time interval $0-\tau_{break}$, plotted as a function of the time interval τ_{break} . The experiment temperatures are 296 K except FeMOF-74 (318 K) and NOTT-300 (293 K). (f) Experimental column breakthrough curve for C_2H_2/C_2H_4 mixed gas containing 1% C_2H_2 over UTSA-100a. Reproduced with permission from Ref. [101]. Copyright 2015 Nature Publishing Group.

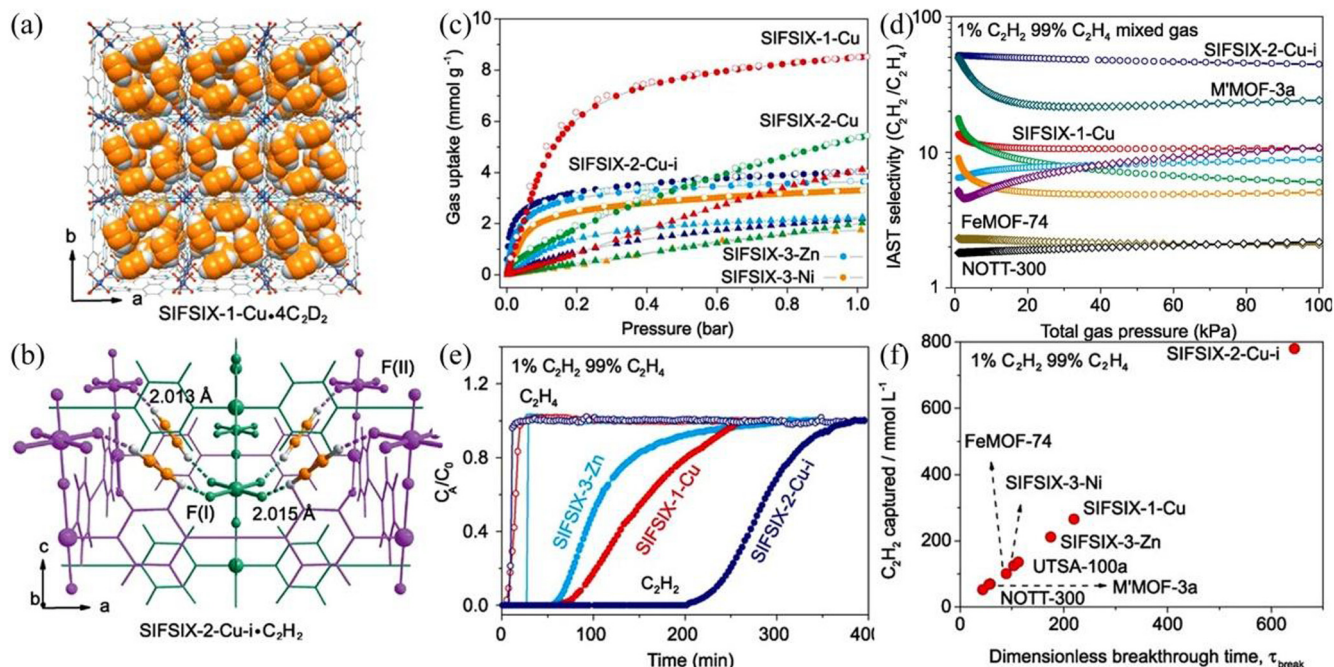


Fig. 7. (a) Neutron crystal structures of SIFSIX-1-Cu \cdot 4C₂D₂ at 200 K from Rietveld analysis. (b) DFT-D-calculated C₂H₂ adsorption binding sites in SIFSIX-2-Cu-i (the different nets are highlighted in magenta and green for clarity), C atoms in C₂H₂ or C₂D₂ are highlighted in orange. (c) Sorption isotherms of C₂H₂ (filled circles) and C₂H₄ (triangles) in SIFSIX-1-Cu (red), SIFSIX-2-Cu (green), SIFSIX-2-Cu-i (blue), SIFSIX-3-Zn (light blue), and SIFSIX-3-Ni (orange) at 298 K, 1.0 bar. Open circles are desorption isotherms of C₂H₂. (d) Comparison of the IAST selectivities of SIFSIX materials versus those of previously reported best-performing materials for 1/99 C₂H₂/C₂H₄ mixtures. (e) Experimental column breakthrough curves for 1/99 C₂H₂/C₂H₄ separations. (f) Plots of the amount of C₂H₂ captured as a function of τ_{break} in the simulated column breakthrough for 1/99 C₂H₂/C₂H₄ separations. Reproduced with permission from Ref. [108]. Copyright 2016 American Association for the Advancement of Science.

the organic ligand layers are pillared by SiF₆²⁻ anions on metal nodes, in which the square-grid sizes can be easily tuned by using various organic linkers of different lengths, giving various MOFs with tunable pore sizes. On the other hand, accessible SiF₆²⁻ anions as hydrogen-bonding donors exposed on the pore surface provide multiple specific sites for acetylene molecules. After optimized investigation, it was found that SIFSIX-2-Cu-i (2 = 4,4'-dipyridylacetylene, i = interpenetrated) shows unprecedentedly high C₂H₂ uptake capacity of 2.1 mmol g⁻¹ at 0.025 bar and 298 K, resulting in record C₂H₂/C₂H₄ selectivities (39.7–44.8) estimated by IAST, which is the most suitable material for the C₂H₄ purification from 1/99 C₂H₂/C₂H₄ mixture (Fig. 7). And SIFSIX-1-Cu (1 = 4,4'-bipyridine) shows the highest C₂H₂ storage capacity of 8.5 mmol g⁻¹ and captured capacity of 6.37 mmol g⁻¹ from 50/50 C₂H₂/C₂H₄ mixture at 1 bar and 298 K, which is most conducive to separate 50/50 C₂H₂/C₂H₄ mixture. High-resolution neutron powder diffraction study of C₂D₂-loaded SIFSIX-2-Cu-i sample showed that acetylene molecule interacts simultaneously with two fluorine atoms from different nets through cooperative C–H \cdots F hydrogen bonds, and there are also van der Waals interactions between acetylene molecules and the organic linkers. For C₂D₂-loaded SIFSIX-1-Cu sample, besides similar types of host–guest interaction as in SIFSIX-2-Cu-i, there are also guest–guest interactions (H^{δ+} \cdots C^{δ-} dipole–dipole interactions) in the cluster of four acetylene molecules. The distinct locations of molecules with different interactions in the pores of SIFSIX well explained the difference in terms of adsorption capacity and selectivity, which were further confirmed by detailed molecular modeling studies. Using first-principles DFT-D calculations, static adsorption energy for acetylene molecule (ΔE) is calculated to be 52.9 and 44.6 kJ mol⁻¹ in SIFSIX-1-Cu and SIFSIX-2-Cu-i, respectively. For ethylene molecules in these SIFSIX materials, their binding strengths are much weaker than acetylene, resulting in highly selective C₂H₂ recognition. Highly efficient separations for C₂H₂/C₂H₄ mixtures

were realized in SIFSIX materials as demonstrated by breakthrough experiments and simulations for two C₂H₂/C₂H₄ mixtures (1/99 and 50/50) that mimic the industrial process conditions. Indeed, trace acetylene impurity can be removed to less than 2 ppm, generating high-purity ethylene. Further breakthrough experiments conducted on the presence of CO₂, moisture and/or O₂ demonstrated well the stability of SIFSIX materials during separation processes. And breakthrough cycling measurements also revealed their good regenerability during many test cycles. By virtue of pore size and chemistry control, these SIFSIX materials show distinct host–guest and guest–guest interactions for acetylene molecules, resulting in extremely high C₂H₂ capture performance, which afford new benchmarks for the highly efficient C₂H₄ purification and C₂H₂ separation from C₂H₂/C₂H₄ mixtures under ambient conditions.

In general, only very few reported porous materials for the separation of C₂H₂/C₂H₄ can fulfill partial sieving effect but not belong to exclusive separation, which means certain co-adsorption of ethylene is unavoidable leading to the waste of partial C₂H₄ production capacity. The ideal C₂H₂/C₂H₄ separation is that only acetylene molecules are adsorbed into porous adsorbents while ethylene molecules are completely blocked outside, generating complete sieving effect. Therefore, it is speculated that the ideal pore aperture size of porous MOFs should be always smaller than the molecular size of C₂H₄ (kinetic diameter: 4.2 Å) but larger than that of C₂H₂ during adsorption processes. On the other hand, the porosity of the adsorbent should be as high as possible to maximize acetylene uptake for high separation productivity. In fact, it is a daunting challenge to design and synthesize such porous MOFs. Very recently, during our exploration on ultramicroporous MOF materials, we discovered a novel SIFSIX material UTSA-300 with pore aperture size of about 3.3 Å and multiple potential binding sites, showing complete C₂H₄ exclusion from the mixture of C₂H₂/C₂H₄ under ambient conditions [109]. UTSA-300 can only

take up acetylene ($76.4 \text{ cm}^3 \text{ g}^{-1}$ at 273 K), but no noticeable ethylene uptake can be observed even at close to its liquefaction temperature. Crystal structures, molecular modeling, selectivity calculation, and experimental breakthrough experiment comprehensively demonstrated this unique material for highly selective $\text{C}_2\text{H}_2/\text{C}_2\text{H}_4$ separation.

2.4. Sulfur dioxide capture

The efficient capture of sulfur dioxide (SO_2) is very important for gas-purification processes including flue-gas desulfurization and natural-gas purification, which can avoid direct detriment on environment and human health or poisoning catalyst. Moreover, trace SO_2 can also inactivate the adsorbents or absorbents for CO_2 removal from flue gas. Therefore, there is a great demand for efficient technologies for trace SO_2 removal from flue gas and other SO_2 -containing gases to replace traditional energy-intensive desulfurization processes. Some early studies have demonstrated that the removal of SO_2 from flue gas can be realized by using many types of adsorbents, especially for high concentration SO_2 . For example, a tetramethylguanidine lactate ionic liquid can absorb SO_2 from 8/92 SO_2/N_2 mixture with capture capacity of 0.305 g g^{-1} at 40°C and 1 bar, while its CO_2 absorption capacity is only of 0.25 wt% [111]. Such chemical absorption is so strong that its desorption can be partially achieved only at very high temperature, as evidenced by the capture capacity of 0.160 g g^{-1} at 94°C , which requires high regeneration energy. Some prussian blues were demonstrated can also take up considerable SO_2 [112]. As revealed by their single component gas sorption isotherms, their adsorption capacity for SO_2 reach to 2.5 mmol g^{-1} , while the CO_2 capacity are up to 1.5 mmol g^{-1} . However, considering the trace amount SO_2 in flue gas (about 2000 ppm), the low SO_2/CO_2 selectivity is unfavourable as the co-adsorption of CO_2 might sacrifice the usage capacity for SO_2 . Thus, high SO_2/CO_2 selectivity is essential for adsorbent materials. In fact, MOFs have been demonstrated as efficient adsor-

bents to address the challenging SO_2 removal, which can capture SO_2 at very low concentration with very high selectivity. Very recently, Chen and Xing et al. comprehensively evaluated hexafluorosilicate (SIFSIX) based MOFs for highly selective recognition of SO_2 from gas mixtures, demonstrating MOFs as superior porous adsorbent for highly efficient removal of trace SO_2 (Fig. 8) [110]. By virtue of pore size tuning (4–10 Å) and multiple binding sites functionalization, SIFSIX materials can exhibit remarkable performance for different gases separation. Typically, SIFSIX materials exhibit a pillared square-grid 3D structure containing 1D pore channels functionalized with hexafluorosilicate F sites. As revealed by X-ray crystal structures and molecular modeling studies, the adsorbed SO_2 molecules interacted with the host frameworks through multiple synergistic host-guest and guest-guest interactions, resulting in stronger binding affinity (highest isosteric adsorption heats of 36–45 kJ/mol). In SIFSIX materials, SO_2 interacts simultaneously with fluorine atoms and pyridine linker through cooperative $\text{S}^{\delta+} \cdots \text{F}^{\delta-}$ electrostatic interactions and $\text{O}^{\delta-} \cdots \text{H}^{\delta+}$ dipole-dipole interactions, accompanied by guest-guest interactions between SO_2 molecules. These strong interactions resulted in highly efficient removal of SO_2 from other gases, even if at a very low SO_2 concentration. At 298 K and 1 bar, SIFSIX-1-Cu showed exceptional and recorded SO_2 uptake capacity of $11.01 \text{ mmol g}^{-1}$. All investigated SIFSIX materials showed remarkable SO_2 uptake capacity even at very low pressure, being consistent with their strong binding affinity to SO_2 molecule as revealed by structural analyses. For example, SIFSIX-2-Cu-i showed unprecedented SO_2 capture capacity of 2.31 mmol g^{-1} at SO_2 partial pressure of 0.002 bar and 298 K under flowed SO_2/N_2 mixed gas, which is equivalent to the concentration of SO_2 in flue gas (2000 ppm). Thus, SIFSIX-2-Cu-i has great potential in flue-gas desulfurization applications. Importantly, these SIFSIX materials showed higher binding affinity and uptake capacity to SO_2 comparing with CO_2 , CH_4 and N_2 , giving recorded SO_2/CO_2 selectivity (86–89) and excellent SO_2/N_2 selectivity (1285–3145), which can ben-

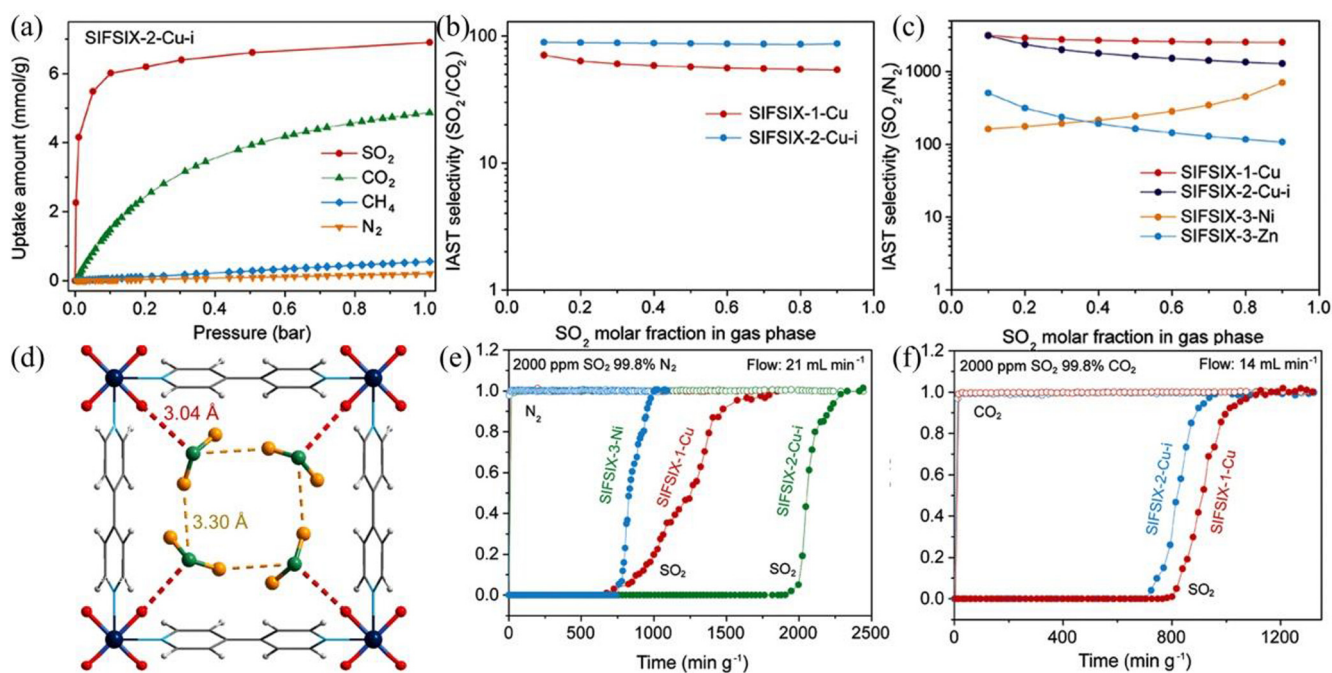


Fig. 8. (a) Adsorption isotherms of SIFSIX-2-Cu-i for SO_2 , CO_2 , CH_4 and N_2 . Note: SO_2 isotherms were measured using SO_2/N_2 mixed gas with varying SO_2 molar fractions under flow mode. CO_2 , CH_4 , and N_2 isotherms were measured using single-component gas. (b–c) IAST selectivities of SIFSIX materials for (b) SO_2/CO_2 and (c) SO_2/N_2 mixtures. (d) Crystal structure obtained from Rietveld refinement of PXRD data on SO_2 -loaded SIFSIX-1-Cu. (e–f) Experimental column breakthrough curves for SO_2/N_2 (2000 ppm SO_2) separations with (e) SIFSIX-1-Cu, SIFSIX-2-Cu-i, and SIFSIX-3-Ni, and SO_2/CO_2 (2000 ppm SO_2) separations and (f) SIFSIX-1-Cu and SIFSIX-2-Cu-i at 298 K and 1.01 bar. Reprinted with permission from Ref. [110]. Copyright 2017 Wiley-VCH.

efit the removal of trace SO₂ during gas desulfurization applications. The remarkable selectivity of these hybrid porous materials was further confirmed by breakthrough experiments with very low SO₂ concentrations, the purification performance is exceptional, stable and regenerable.

The excellent performance reported in this study sets a new benchmark in the highly efficient removal of trace SO₂ from flue gas or natural gas using porous materials, which reveals a path forward for industrial related separations.

2.5. Carbon dioxide capture

The environmental and energy concern of carbon dioxide emission (as a major greenhouse gas) has drawn unprecedented attention to develop applicable and efficient technologies for carbon dioxide capture and separation. To capture carbon dioxide from flue gas, aqueous amine-based absorbents are applied on large scale to chemically adsorb it during practical process. However, the regeneration of these chemisorbents is usually carried out at high temperatures due to their extremely high CO₂ affinity and poor reversibility, which is highly energy-intensive. Also, this technology can cause the corrosion of equipment and pipelines. In contrast, reversible CO₂ sorption using physisorbents such as MOFs is more energy-efficient. And, the exceptional uptake capacities of MOFs for CO₂ storage at room temperature demonstrate that they can serve as good candidates during related process [113]. Compared with CO₂, the other components of different gas mixtures (natural gas, flue gas etc.) like CH₄ and N₂ show different physical properties (polarizability $\times 10^{25}/\text{cm}^3$: CO₂ 29.1, CH₄ 25.9 and N₂ 17.4; quadrupole moment $\times 10^{40}/\text{C}\cdot\text{m}^2$: CO₂ 13.4, CH₄ 0 and N₂ 4.7). In general, the higher polarizability and quadrupole moment of CO₂ result in stronger interactions with the pore surface of

MOFs, which can be further enhanced by incorporating polar functional sites, showing great potential in CO₂ capture and separation [68,69]. In fact, most MOFs for CO₂ separation belong to this type of thermodynamic separation. For those MOFs without explicit binding site, the relatively similar kinetic diameters of these molecules (CO₂ 3.30, CH₄ 3.76 and N₂ 3.64 Å) require the precisely tuning of their pore size for molecular sieving, which is a highly challenging task.

As mentioned earlier, interpenetration strategies are powerful to easily obtain MOFs with tunable pore sizes, which can realize selective recognition of CO₂ from CH₄ and N₂. The evaluation of CO₂/N₂ and CO₂/CH₄ separation did not involve breakthrough fixed-bed experiment until in 2008 [114]. Bastin et al. demonstrated that the double interpenetrated [Zn₂(bdc)₂(bpy)], described above with suitable pore size of about 4.0 Å, can fulfill the capture and separation of CO₂ from its binary and ternary mixtures (Fig. 9). The pore size of MOF-508 is similar to the molecular sizes of CO₂, CH₄ and N₂ (3.30, 3.76 and 3.64 Å, respectively), but still allow diffusion of these three gas molecules to its confined space with considerable host-guest interaction. Single-component adsorption isotherms revealed that the adsorption capacities of MOF-508b for CO₂, CH₄ and N₂ are 26.0, 5.5 and 3.2 wt%, respectively, at 4.5 bar and 303 K. The adsorption enthalpy at zero coverage for CO₂ is determined to be 14.9 kJ mol⁻¹, which is much higher than those for CH₄ and N₂. The potential of the MOF for CO₂ capture and separation were checked first by single-component breakthrough experiments, resulting in a breakthrough time hierarchy of CO₂ > CH₄ > N₂. All these results clearly confirm that CO₂ is highly preferentially adsorbed by MOF-508b over CH₄ and N₂. Further breakthrough fixed-bed experiments indicated that CO₂ can be efficiently removed from its binary CO₂/CH₄ and CO₂/N₂ and ternary CH₄/N₂/CO₂ mixtures, giving CO₂/CH₄ selectivity of 3 and CO₂/

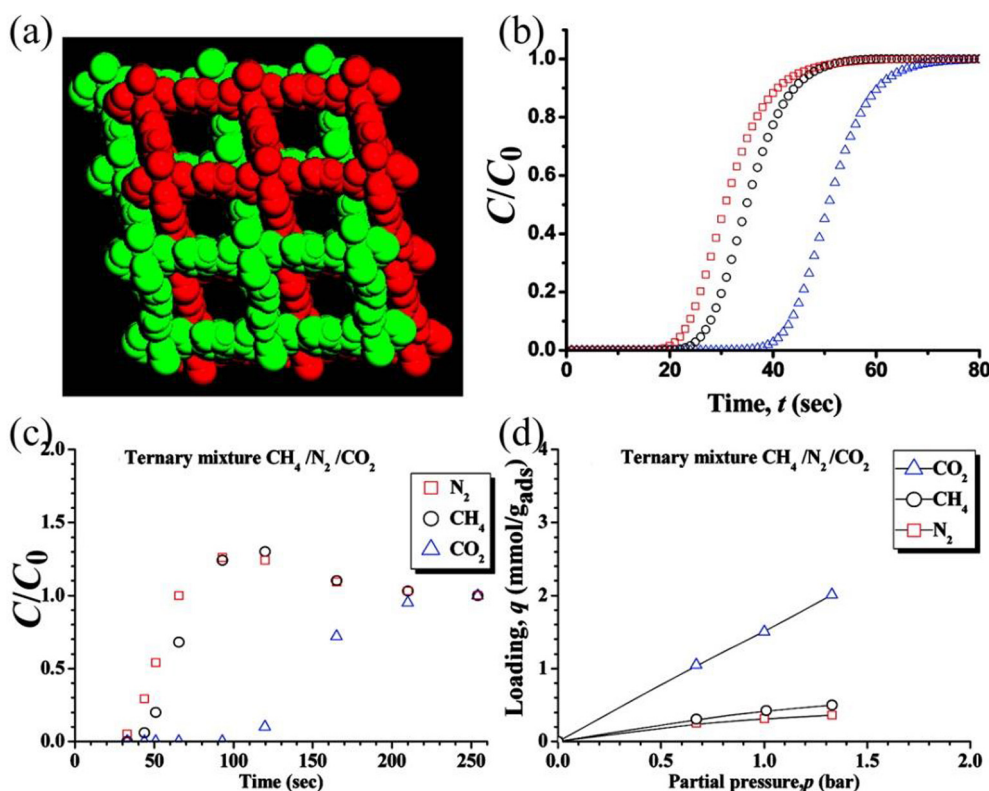


Fig. 9. (a) One-dimensional micropores of about 4.0 Å × 4.0 Å in MOF-508. (b) Single-component breakthrough curves for N₂ (square), CH₄ (circle), and CO₂ (triangle) at 323 K and 1 bar. (c) Multicomponent breakthrough curves for equimolar ternary mixture of CH₄/N₂/CO₂ at 303 K and 1 bar. (d) Adsorption isotherms for equimolar ternary mixture of CH₄/N₂/CO₂ at 303 K. Lines are to guide the eye. Reprinted with permission from Ref. [114]. Copyright 2008 American Chemical Society.

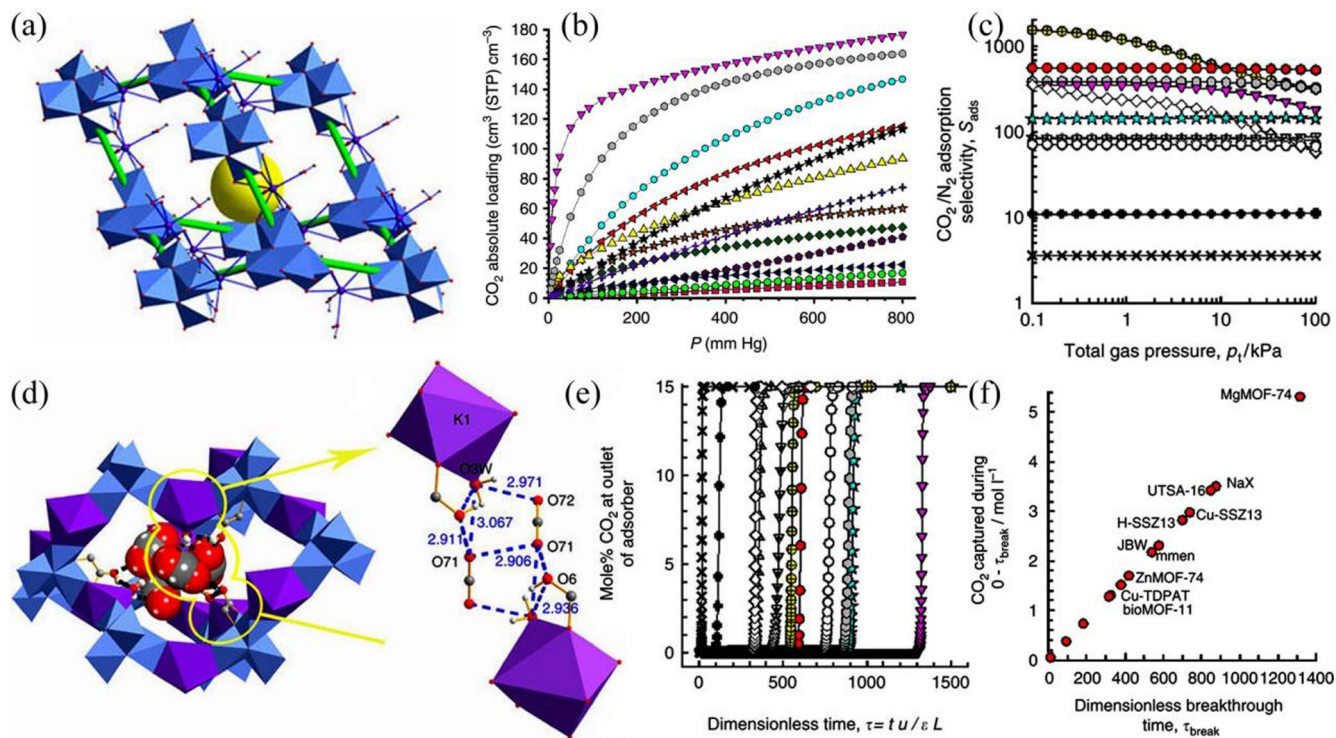


Fig. 10. (a) The cavity structure of UTSA-16 (yellow ball of about 4.5 Å in diameter). The linkages between the cubic clusters are present with the green sticks to illustrate the framework topology. (b) Comparison of the adsorption isotherms of CO₂ at 296 K. From top to bottom, The considered MOFs are MgMOF-74 (magenta down triangle), UTSA-16 (gray hexagon), ZnMOF-74 (cyan circle), bio-MOF-11 (red left triangle), CuBTC (black star), Cu-TDPAT (yellow up triangle), UTSA-20a (violet cross), ZIF-78 (orange star), Zn₅(BTA)₆(TDA)₂ (olive diamond), Zn(bdc)(dabco) (purple pentagon), MIL-101 (navy left triangle), Yb(BPT) (green hexagon) and MOF-177 (pink square). (c) Calculations using Ideal Adsorbed Solution Theory (IAST) for CO₂/N₂ adsorption selectivity. The considered materials are MgMOF-74 (purple down triangle), NaX (cyan star), UTSA-16 (gray hexagon). (d) A couple of CO₂ dimers are trapped within the cage and the cooperative interactions between CO₂ molecules and the framework. (e) Simulated breakthrough curves for 15/85 CO₂/N₂ mixture in an adsorber packed with different adsorbents and maintained at isothermal conditions at 296 K. (f) Plot of the number of moles of CO₂ captured from CO₂/N₂ mixture per litre of adsorbent material. Reproduced with permission from Ref. [115]. Copyright 2012 Nature Publishing Group.

N₂ selectivity of 6 as estimated from breakthrough experiments. This is the first example of porous MOFs for the real separation of CO₂ from CH₄ and N₂ in their binary and ternary mixtures, using fixed-bed breakthrough to mimic practical separation process. Since then, this challenging technology has gradually become a metrics to evaluate MOFs for CO₂ separation.

Later, extensive research endeavours on functionalized MOFs for CO₂ separation demonstrated that open metal sites (OMSs) [116–121], specific polar groups (–NH₂, –OH, etc.) [122–129] or pore size controlling are efficient in improving CO₂ separation performance [130–138]. Ideally, immobilization of specific functional sites in MOFs can afford preferential binding sites for CO₂, and simultaneously optimizing the pore/cage sizes can maximize the van der Waals interactions between the pore surfaces and CO₂. Such dual-functionality collaboratively results in high separation selectivity and capacity, realizing optimal CO₂ capture applications at ambient conditions [102]. During our exploration ultramicroporous MOF materials, we targeted a very special MOF [K(H₂O)₂–Co₃(cit)(Hcit)] (UTSA-16) from a very cheap chemical citric acid (Hcit) to exhibit remarkable performance for carbon capture [115]. UTSA-16 is a three-dimensional framework with dia topology, which is composed of Co₄O₄ clusters and K⁺-polyhedra linkers via face-sharing and further infinite three-dimensional heteronuclear M–O–M connections. UTSA-16 contains three-dimensional channels of about 3.3 × 5.4 Å² and small cavities of 4.5 Å (Fig. 10), exhibiting considerable BET surface area of 628 m² g^{−1}. The activated UTSA-16 exhibited high CO₂ uptake of 160 cm³ cm^{−3}, high CO₂/CH₄ selectivity (29.8) for 50/50 CO₂/CH₄ mixture and CO₂/N₂ selectivity (314.7) for 15/85 CO₂/N₂ mixture at ambient conditions, which are higher than those of most MOFs used

for comparison. Simulated breakthrough experiments to evaluate the CO₂ capture performance in fixed-bed adsorber further confirm that UTSA-16 exhibits high CO₂ adsorption capacity and selectivity for binary CO₂/CH₄ and CO₂/N₂ gas mixtures. Powder neutron diffraction studies demonstrated that remarkable performance of UTSA-16 for CO₂ capture can be attributed to its optimal pore size and suitable binding sites for CO₂ (bind on the terminal coordinated water molecules through hydrogen bonding interactions). Such air-stable UTSA-16 synthesized from cheap raw materials enables it a potential candidate for CO₂ capture and removal.

Hereafter, research endeavours from different researchers realized benchmarks in the highly efficient capture of CO₂ using porous materials, facilitating practical application of this type of adsorbents [139]. To evaluate different solid adsorbents for CO₂ capture under realistic conditions, Long et al. and Zaworotko et al. carried out equilibrium sorption experiments of gas mixtures including CO₂, N₂, and H₂O, respectively, using some representative MOFs, mesoporous silicas, zeolites and activated carbons that have received great attention for CO₂ capture [140,141]. The amine-modified chemisorbents can keep their exceptional performance moist CO₂ stream although their adsorption heats are unfavourable for regeneration. Another approach is using water stable ultramicroporous MOFs. For example, Eddaoudi et al. demonstrated that NbOFFIVE-1-Ni can maintain its CO₂ uptake capacity of about 2.2 mmol g^{−1} even after 6 months immersion in water [142]. Under humid condition (74% RH), the CO₂ capture capacity of NbOFFIVE-1-Ni for 1/99 CO₂/N₂ mixture slightly decrease from 8.2 wt% to 5.6 wt%. By virtue of versatile functionalization strategies, the pore surface and size can be simultaneously controlled. Taking related factors during CO₂ capture into account (selectivity,

adsorption capacity and kinetics, regeneration conditions, material stability, impurity tolerance, economic cost...) [63], designed MOFs can be competent for CO₂ separation over a wide concentration range, being targeted to apply in flue gas treatment, natural gas processing, trace CO₂ removal in confined spaces, and air capture.

2.6. Separations of C₂H₂/CO₂

Acetylene (C₂H₂) is an important source of many chemical products including acrylic acid derivatives, vinyl compounds, and α -ethynyl alcohols in the chemical industry since its can undergo a variety of addition reactions. Accordingly, the production of high purity acetylene is of great industrial significance. The big challenge is the coexisting of CO₂ impurity during the production of C₂H₂, while C₂H₂ and CO₂ have almost identical sizes, shapes (3.32 × 3.34 × 5.70 and 3.18 × 3.33 × 5.36 Å³, respectively), and physical properties (boiling points of 189.3 and 194.7 K, respectively). Therefore, the exploitation of efficient physical C₂H₂ adsorbent is highly demanded. In general, immobilized functional sites in porous adsorbents can maximize the tiny difference between C₂H₂ and CO₂, leading specific recognition of these similar gas molecules. Open metal sites and electronegative Lewis base sites are demonstrated to be effective for enhancing the C₂H₂ binding affinity. Structurally, for electronegative Lewis base sites, C₂H₂ can bind to it as H-donor through hydrogen-bonding interaction, while CO₂ only interacts with its electropositive carbon through weaker electrostatic interaction. For open metal sites, C₂H₂ binds to it with pi system through stronger coordination bond, while CO₂ coordinates to metal site using its electronegative O atoms. The first example using MOF for selective adsorption of C₂H₂ over CO₂ was realized by Kitagawa et al. in 2005 [143]. They synthesized an ultramicro-porous material with one-dimensional channels (4 Å × 6 Å) that

can accommodate C₂H₂ well via strong hydrogen-bonding interactions, showing considerable C₂H₂/CO₂ separation. Later, by virtue of unique kinetically controlled flexibility, Zhang and Chen reported a dynamic porous material for high C₂H₂/CO₂ separation performance, in which unprecedented C₂H₂ hexamer was found binding to electronegative N atoms via hydrogen-bonding interactions [144]. During the last several years, C₂H₂/CO₂ separations have been realized for a few more MOFs [145–152], and even for the first time employing a porous hydrogen-bonded organic framework HOF-3 to address such a separation [153].

Particularly, Luo, Chen and co-authors reported a novel MOF-74 isomer [Zn₂(dobdc)(H₂O)]·0.5H₂O (Zn-UTSA-74, H₄dobdc = 2,5-dioxido-1,4-benzenedicarboxylic acid) with two accessible binding sites per metal center for high C₂H₂/CO₂ separation. Zn-UTSA-74 has novel four connected **fgl** topology with one-dimensional open channels of about 8.0 Å [154]. Unlike open metal sites in the well established MOF-74 that each metal center is in a five coordinate square pyramidal coordination geometry with only one open side, there are two different Zn centers within the binuclear secondary building units in Zn-UTSA-74, in which one Zn is in a tetrahedral while the other one in octahedral coordination geometry. After activation, the two axial water molecules on six-coordinated zinc centers can be removed, generating Zn-UTSA-74a with two accessible binding sites per Zn ion for gas molecules (Fig. 11). With the same open metal sites, Zn-UTSA-74a took up a moderately high and comparable amount of acetylene (145 cm³ cm⁻³) to Zn-MOF-74. X-ray crystal structures and molecular modeling studies revealed that open zinc sites bind with two C₂H₂ molecules per metal site and one molecule per metal site for CO₂, respectively. Interestingly, the accessible open zinc sites in Zn-UTSA-74a are bridged by CO₂ molecules rather than taking terminal-binding mode in Zn-MOF-74, so Zn-UTSA-74a adsorbs a much smaller amount of CO₂ (90 cm³ cm⁻³) than Zn-MOF-74 (146 cm³ cm⁻³) at

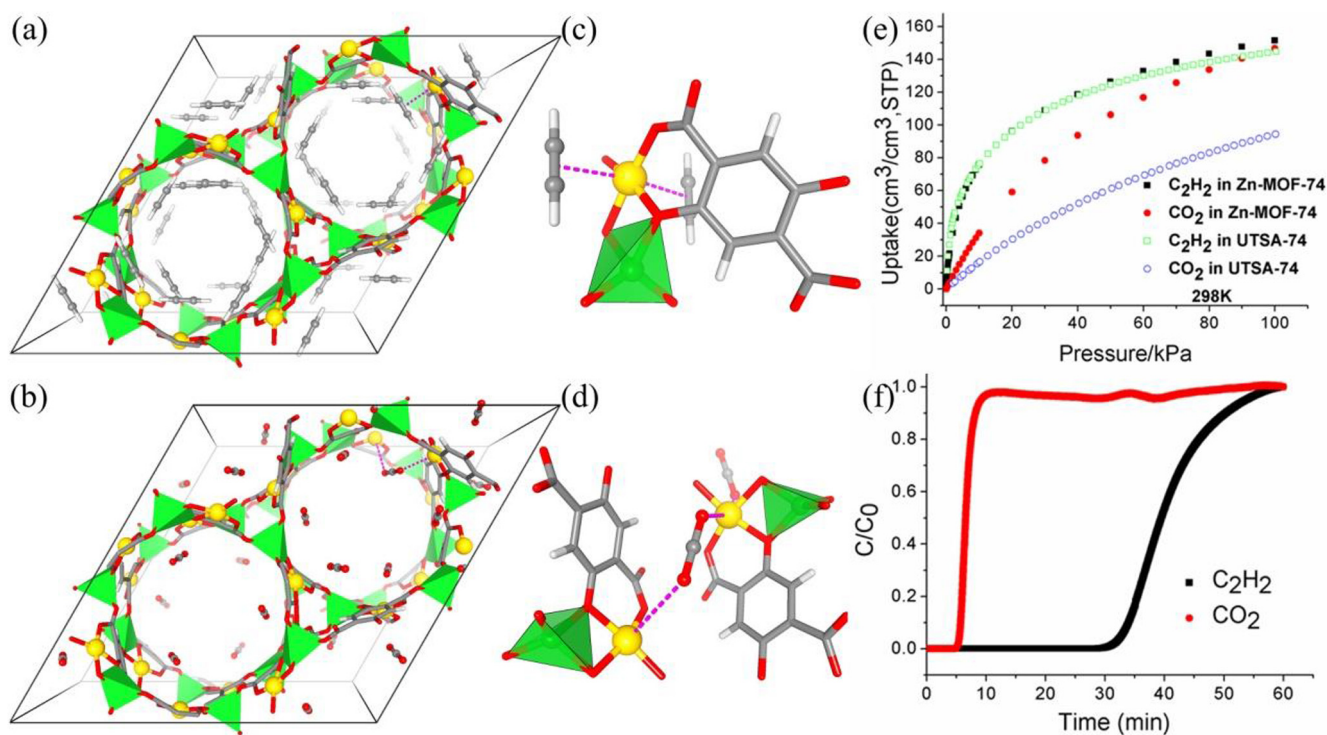


Fig. 11. (a) DFT-D optimized structure of UTSA-74⊃C₂H₂, (b) X-ray single crystal structure of UTSA-74⊃CO₂ and (c–d) their corresponding local coordination environments. The Zn ions with two accessible binding sites are highlighted in gold, and the tetrahedral ions are shown in green tetrahedron. (e) Comparison of sorption isotherms of C₂H₂ and CO₂ for UTSA-74 and Zn-MOF-74 at 298 K. (f) Experimental column breakthrough curve for an equimolar C₂H₂/CO₂ mixture (298 K, 1 bar) in an adsorber bed packed with UTSA-74a. Reproduced with permission from Ref. [154]. Copyright 2016 American Chemical Society.

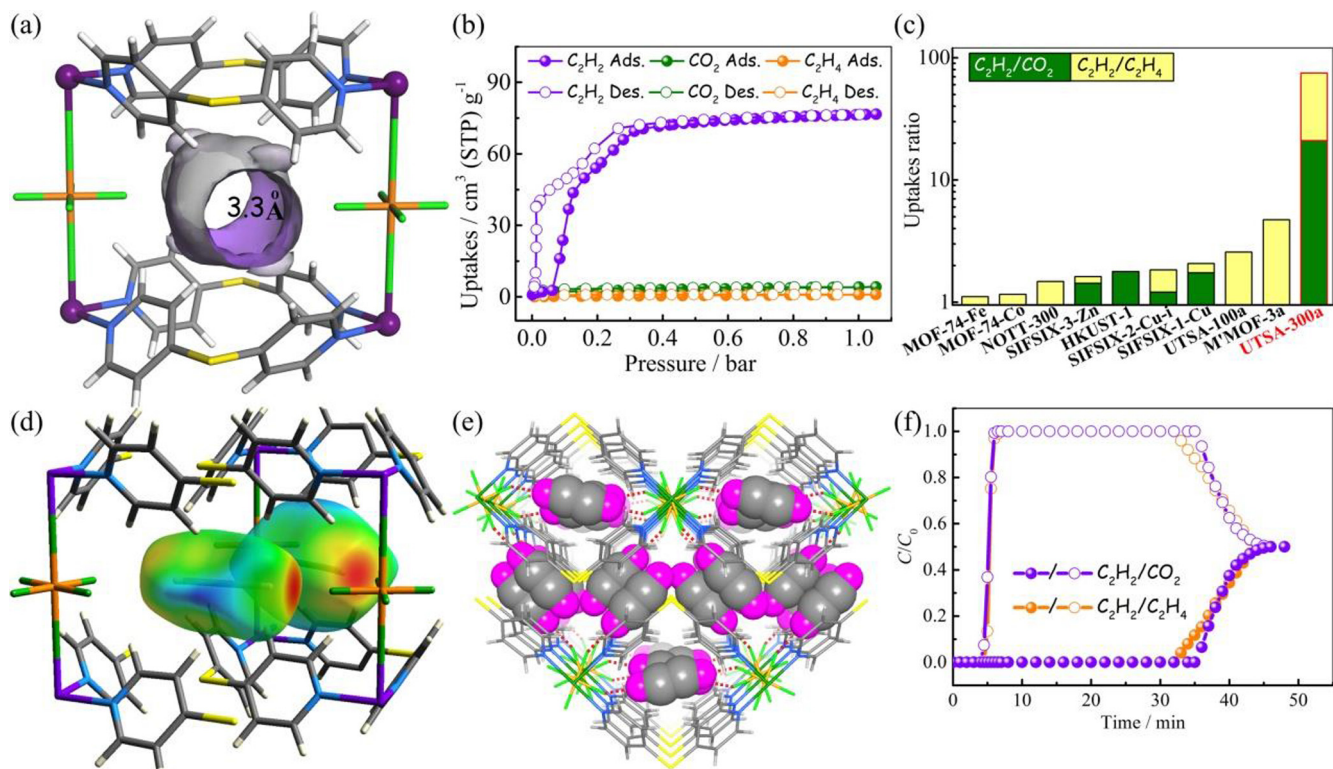


Fig. 12. (a) Perspective views of cage unit in UTSA-300 showing aperture size of 3.3 Å (Zn, Si, F, S, N, and C are represented by purple, orange, green, bright yellow, light blue, and gray, respectively, and solvent molecules are omitted for clarity). (b) C_2H_2 , CO_2 , and C_2H_4 single-component sorption isotherms for UTSA-300a at 273 K. (c) Comparison of uptakes ratio among UTSA-300a and representative MOFs at ambient conditions. (d) Preferential binding sites in UTSA-300 for C_2D_2 molecules shown with Hirshfeld surface (d_i) displaying C–D···F interactions (red area). (e) Packing diagram of UTSA-300 $\supset C_2D_2$ from neutron powder diffraction data, C_2D_2 molecules are shown in a CPK model. (f) Experimental column breakthrough curves for equimolar C_2H_2/CO_2 (purple) and C_2H_2/C_2H_4 (orange) mixtures (298 K, 1 bar) in an adsorber bed packed with UTSA-300a. C_0 is the total concentration of gases at outlet. Reproduced with permission from Ref. [109]. Copyright 2017 American Chemical Society.

room temperature and ambient pressure, leading to a superior MOF material for high C_2H_2/CO_2 separation. Also, Zn-UTSA-74a exhibits higher isosteric adsorption heats for C_2H_2 than that of CO_2 (31 and 25 kJ mol^{-1} , respectively), which certainly higher than those of Zn-MOF-74. Experimental breakthrough supports complete separation of C_2H_2 from the equimolar C_2H_2/CO_2 mixture by a Zn-UTSA-74a column. This is the first example of porous MOFs whose C_2H_2/CO_2 separation performance has been clearly established by experimental breakthrough. Notably, this MOF will become another promising prototypical MOF for molecular recognition and chemical transformations.

Although binding sites like open metal sites are powerful for selective C_2H_2/CO_2 separations, none of porous materials has been targeted to exhibit complete exclusion of CO_2 from C_2H_2 based on physical sorption. Ideal porous materials for C_2H_2/CO_2 separation are those only take up one component while completely excluded the other one. In order to develop microporous materials for complete sieving effects for such a challenging separation, we need to not only fine-tune the pore sizes to match the molecular sizes of these two gas molecules of about 3.3 Å but also introduce some specific sites to bind C_2H_2 molecules exclusively. Very recently, we realized complete CO_2 exclusion from C_2H_2 under ambient conditions in novel microporous material [Zn(dps) $_2$ (SiF $_6$)] (UTSA-300, dps = 4,4'-dipyridylsulfide) that contains multiple potential binding sites and a pore aperture size of about 3.3 Å (Fig. 12) [109]. This MOF is composed of cage-like units with hexafluorosilicate F sites generating two dimensional networks with undulating 2D channels. The structure exhibits a pore open-close transformation during activation/desolvation, giving a closed-pore framework UTSA-300a with dispersed OD cavities after conformation change

of the pyridyl ligand and rotation of SiF $_6^{2-}$ pillars. Strong C–H···F and π – π stacking interactions are found in closed-pore UTSA-300a, blocking the pore aperture and stabilizing the dynamic structure. Apparently, the pore aperture size (about 3.3 Å) of UTSA-300 allows inward diffusion of both CO_2 and C_2H_2 . However, gas sorption studies indicated that UTSA-300a shows exceptional C_2H_2/CO_2 selectivity under ambient conditions, which can only adsorb acetylene (76.4 $\text{cm}^3 \text{g}^{-1}$) while no adsorption was observed for carbon dioxide. Hence, its uptake ratio of C_2H_2/CO_2 is unprecedentedly higher than any other porous MOF materials. Neutron powder diffraction and molecular modeling studies clearly revealed that acetylene molecule primarily binds to two hexafluorosilicate F atoms of UTSA-300a via strong C–H···F interactions, which broke the original intranetwork hydrogen bond and subsequently expanded to its open-pore structure. The material showed highest binding affinity for C_2H_2 with an isosteric heat of adsorption of 57.6 kJ mol^{-1} , promoting the transformation to open-pore structure and subsequently stabilizing it. The C_2H_2/CO_2 selectivity calculated from IAST for a binary equimolar mixture reached to 743 at 298 K and 1 bar. The remarkable selectivity was further confirmed by breakthrough experiment using a flowing 50/50 C_2H_2/CO_2 mixture at 1 bar and 298 K. UTSA-300a is highly efficient for C_2H_2/CO_2 separation, giving high purity single gas component during the dynamic separating process. Clearly, as revealed by acetylene-loaded structure, C_2H_2 can stably interact with the electrostatic potential around SiF $_6^{2-}$, resulting the pore opening. On the other hand, for CO_2 , the same binding mode as C_2H_2 would result in repulsive interactions because of the opposite quadrupole moment, thus failing to open the pore structure under ambient conditions and showing no adsorption uptake. Strong binding sites

in confined space of ultra-microporous MOFs can effectively recognize different molecules with identical size and shape based on different binding modes. To date, such complete molecular exclusion of CO_2 from C_2H_2 was observed only in this novel MOF molecular sieve.

The above endeavours realized excellent $\text{C}_2\text{H}_2/\text{CO}_2$ separation that sets a new benchmark in separation of greatly challenging molecules with very similar sizes and physical properties, which will facilitate the design and implementation of more novel MOF materials for other important gas separations.

2.7. Separations of $\text{C}_3\text{H}_4/\text{C}_3\text{H}_6$

Propylene is one of most important chemical feedstocks (over 120 million tons produced in 2016), which is mainly produced by cracking larger hydrocarbon molecules in oil refining. The raw propylene product contains trace amounts of propyne, an undesirable byproduct, which can highly interfere with the catalytic polymerization of propylene. The concentration of propyne during polymerization of propylene should meet the requirement of below 5 ppm. Hence, the removal of trace amounts of propyne from propylene is essential for the production of polymer-grade propylene. Traditionally, cryogenic distillation or catalytic partial hydrogenation is applied to remove/transform propyne to an acceptable level. As an improved alternative, adsorptive gas impurity capture using porous materials is more environmentally friendly and energy-efficient, and it can also better utilize propyne to other applications. Except the work by our group, there is no previously reported example of using porous material for adsorptive separation of propyne from propylene so far. Probably, compared with acetylene/ethylene, the differences of molecular sizes/shapes (kinetic diameters: C_3H_4 , ~ 4.76 Å; C_3H_6 , ~ 4.68 Å)

and physical/chemical properties between propyne and propylene is smaller than those of acetylene/ethylene, making propylene purification a great challenge.

Very recently, Li and Chen et al. reported the first example of flexible-robust metal-organic frameworks capable of fulfilling this challenging $\text{C}_3\text{H}_4/\text{C}_3\text{H}_6$ separation [155]. ELM-12 consists of a rigid square-grid copper bipyridine scaffold with dynamic dangling OTf⁻ groups. After sample activation, ELM-12 can show porosity (void = 20.5%, pore volume = $0.141 \text{ cm}^3 \text{ g}^{-1}$) with two kinds of cavities (I and II, Fig. 13). These cavities ($6.1 \text{ \AA} \times 4.3 \text{ \AA} \times 4.3 \text{ \AA}$ and $6.8 \text{ \AA} \times 4.0 \text{ \AA} \times 4.2 \text{ \AA}$) match well with the size and shape of C_3H_4 ($6.2 \text{ \AA} \times 3.8 \text{ \AA} \times 3.8 \text{ \AA}$, compared with $6.5 \text{ \AA} \times 4.0 \text{ \AA} \times 3.8 \text{ \AA}$ for C_3H_6). The C_3H_4 adsorption capacity of ELM-12 reaches to 2.55 mmol/g at 0.1 bar and 298 K, while the C_3H_6 adsorption capacity is only 0.67 mmol/g , exhibiting strong interactions with propyne as confirmed by the isosteric heats of adsorption (60.6 kJ mol^{-1}). Such uptake difference not only benefits for C_3H_6 purification but also breaks the stereotype that flexible MOFs are inferior for gas separation. The IAST selectivity of ELM-12 for 1/99 $\text{C}_3\text{H}_4/\text{C}_3\text{H}_6$ mixture was estimated to be 84. These outstanding adsorption and separation performance were supported well by neutron powder diffraction of C_3D_4 -loaded sample, showing that propyne interacts simultaneously with two oxygen atoms of OTf⁻ groups from different nets through cooperative C–H \cdots O hydrogen bonds. Density functional theory (DFT-D) calculations showed the binding affinity of C_3H_6 in ELM-12 (binding energies E_B only $\sim 32.3 \text{ kJ/mol}$) is significantly lower than that of C_3H_4 , well explaining that the high $\text{C}_3\text{H}_4/\text{C}_3\text{H}_6$ adsorption selectivity originates from the strong binding of C_3H_4 with the polar OTf⁻ groups. The remarkable separation performance of ELM-12 was confirmed using breakthrough experiments conducted on two $\text{C}_3\text{H}_4/\text{C}_3\text{H}_6$ mixtures (1/99 and 50/50) to mimic the industrial process conditions. The trace C_3H_4 was effi-

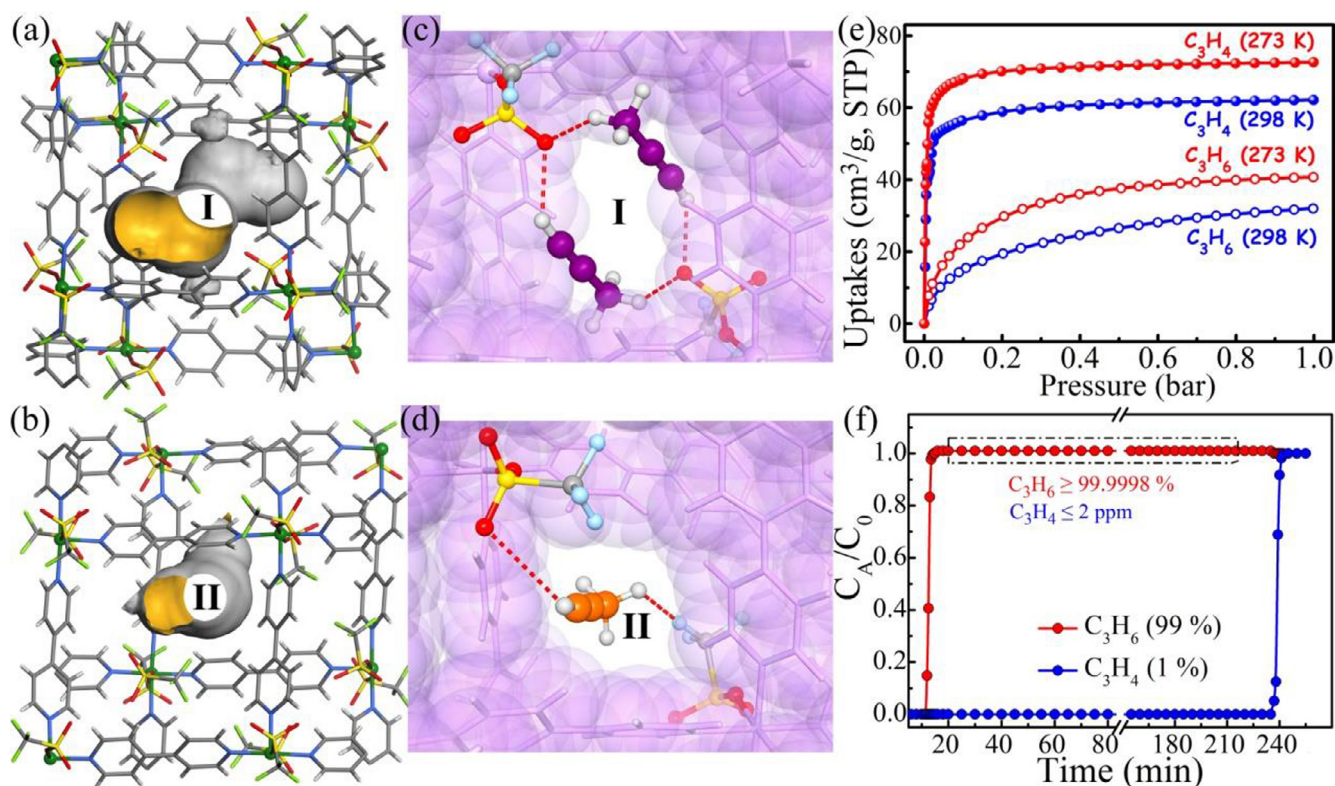


Fig. 13. (a, b) Schematic diagrams of the two types of cavities (I and II) in ELM-12 (Cu, green; C, gray; O, red; S, yellow; F, light green). (c, d) Neutron diffraction crystal structure of ELM-12- C_3D_4 showing the preferential binding sites for C_3D_4 molecules (sites I and II) and their close contacts with the framework. (e) C_3H_4 and C_3H_6 adsorption isotherms of ELM-12 at ambient conditions. (f) Experimental column breakthrough curves for a $\text{C}_3\text{H}_4/\text{C}_3\text{H}_6$ mixture containing 1% C_3H_4 (298 K, 1.01 bar) in an absorber bed packed with ELM-12. Reproduced with permission from Ref. [155]. Copyright 2017 American Chemical Society.

ciently removed from C₃H₆ in the fixed bed to yield a polymer-grade C₃H₆ (>99.9998%). Additional experiments indicated that the presence of C₃H₈, C₂H₄, and CO₂ has no effect on the separation of C₃H₄ from C₃H₆. It is worth noting that ELM-12 also shows good regenerability and stability even after two years aging. Remarkably, the high efficiency of ELM-12 to remove the trace C₃H₄ from raw C₃H₄/C₃H₆ mixtures under ambient conditions makes this MOF a practically promising adsorbent for this important separation.

3. Conclusion and outlook

In this review, we have summarized our ongoing research endeavours during the exploration and discovery of microporous MOFs for efficient separation and purification of some important gas mixtures, including breakthroughs on the gas chromatographic separation of hexane isomers, kinetic separation of hydrogen isotope, acetylene/ethylene separation, carbon dioxide capture, acetylene/carbon dioxide and propylene/propyne separation. Also, several successful strategies to construct promising MOFs for unprecedented discoveries also have been outlined. Theoretically speaking, based on an infinite number of metal ions and organic linkers, metal-organic frameworks can be customized to have unlimited possible pore structures and physical/chemical functionalities. Therefore, we can readily design and synthesize MOFs with desired porosities, surface areas, pore sizes, and functional sites for challenging gas separation and purification. Intensive efforts have demonstrated that the separation performance of metal-organic frameworks for important gas mixtures can be far beyond our initial imagination, which in turn confirms that MOFs are one of the most promising and variable platforms to develop functional materials. Notably, at the early stage of exploring functional MOFs for gas separation, overall gas uptakes and derived gas selectivities from single-component isotherms were simply used to assess the separation performance. However, such static sorption is not applicable to practical dynamic systems. Fortunately, the application of some powerful technologies including chromatographic separation, fixed-bed adsorption and/or breakthrough experiments has facilitated the expansion of research interests on MOFs into industrial applications. Indeed, strong progresses in important gas separation have been made under great research endeavours on pore and function engineering of MOFs. However, before the implementation of industrial and commercial usage for the separation and purification of small gas molecules, it should be noted that there are still many issues remaining to be addressed, which requires chemists and engineering scientists of different expertise and industrial partners to work cooperatively. In realistic separation systems, the gas mixtures and operation conditions are more complicated. Many factors need to be taken into account for MOFs to perform successfully under industrially relevant conditions, including adsorption kinetics, mechanical properties, impurity tolerance, regeneration, and so on, because of the actual application requirement of pelleting or films/membranes fabrication. Among these indices, the stability of MOF materials including durability and repeatability is a key factor in achieving industrial separation application. As summarized above, there are some MOF adsorbents that show remarkable tolerance for impurity including humidity, which have been studied under simulated condition as practical application. In addition, those stable MOFs with high performance need to be further comprehensively investigated for their practical gas separation and purification. Notably, efficient MOF adsorbents obtained from raw materials of cheap cost by using simple and environmental-friendly synthesis method are the most favourable materials. Close collaboration with industrial partners can significantly facilitate such a very important process to implement those

potential MOF materials for industrial gas separation and purification. Although some progress in films/membranes fabrication has been made after efforts from a few groups, there are new challenges emerging to be addressed, such as membrane defects, low permeability, poor processability and scaling up the membranes. These major hurdles prevent membranes to be used for bulk separation, which also means tremendous opportunity not only for academic researchers but also for industrial partners. Overall, the full spectrum of separations technologies with energy efficient prospects needs to be broadened. Considering more efforts from the MOF community being put into this exciting area, future studies aiming to better and cheaper approaches to separate mixtures of chemicals are believed to reap great global benefits.

Acknowledgement

This work was supported by Grant AX-1730 from the Welch Foundation (B.C.) and the National Natural Science Foundation of China (H.X.; No. 21436010).

Appendix A. Supplementary data

Supplementary data associated with this article can be found, in the online version, at <https://doi.org/10.1016/j.ccr.2017.09.027>.

References

- [1] H.H. Wu, Q.H. Gong, D.H. Olson, J. Li, *Chem. Rev.* 112 (2012) 836–868.
- [2] Z.R. Herm, E.D. Bloch, J.R. Long, *Chem. Mater.* 26 (2014) 323–338.
- [3] Z. Bao, G. Chang, H. Xing, R. Krishna, Q. Ren, B. Chen, *Energy Environ. Sci.* 9 (2016) 3612–3641.
- [4] J.-R. Li, R.J. Kuppler, H.-C. Zhou, *Chem. Soc. Rev.* 38 (2009) 1477–1504.
- [5] J.R. Li, J. Sculley, H.C. Zhou, *Chem. Rev.* 112 (2012) 869–932.
- [6] K. Sumida, D.L. Rogow, J.A. Mason, T.M. McDonald, E.D. Bloch, Z.R. Herm, T.H. Bae, J.R. Long, *Chem. Rev.* 112 (2012) 724–781.
- [7] S. Qiu, M. Xue, G. Zhu, *Chem. Soc. Rev.* 43 (2014) 6116–6140.
- [8] K. Adil, Y. Belmabkhout, R.S. Pillai, A. Cadiau, P.M. Bhatt, A.H. Assen, G. Maurin, M. Eddaoudi, *Chem. Soc. Rev.* 46 (2017) 3402–3430.
- [9] D.S. Sholl, R.P. Lively, *Nature* 532 (2016) 435–437.
- [10] H. Furukawa, K.E. Cordova, M. O’Keeffe, O.M. Yaghi, *Science* 341 (2013) 123044.
- [11] H.-L. Zhou, Y.-B. Zhang, J.-P. Zhang, X.-M. Chen, *Nat. Commun.* 6 (2015) 6917.
- [12] Y.-B. Zhang, H. Furukawa, N. Ko, W. Nie, H.J. Park, S. Okajima, K.E. Cordova, H. Deng, J. Kim, O.M. Yaghi, *J. Am. Chem. Soc.* 137 (2015) 2641–2650.
- [13] S. Yuan, Y.-P. Chen, J.-S. Qin, W. Lu, L. Zou, Q. Zhang, X. Wang, X. Sun, H.-C. Zhou, *J. Am. Chem. Soc.* 138 (2016) 8912–8919.
- [14] Q.-G. Zhai, X. Bu, C. Mao, X. Zhao, L. Daemen, Y. Cheng, A.J. Ramirez-Cuesta, P. Feng, *Nat. Commun.* 7 (2016) 13645.
- [15] Y. He, W. Zhou, G. Qian, B. Chen, *Chem. Soc. Rev.* 43 (2014) 5657–5678.
- [16] B. Li, H.-M. Wen, H. Wang, H. Wu, M. Tyagi, T. Yildirim, W. Zhou, B. Chen, *J. Am. Chem. Soc.* 136 (2014) 6207–6210.
- [17] B. Li, H.-M. Wen, W. Zhou, Jeff Q. Xu, B. Chen, *Chem* 1 (2016) 557–580.
- [18] M.K. Taylor, T. Runčevski, J. Oktawiec, M.I. Gonzalez, R.L. Siegelman, J.A. Mason, J. Ye, C.M. Brown, J.R. Long, *J. Am. Chem. Soc.* 138 (2016) 15019–15026.
- [19] R.-B. Lin, B. Chen, *IUCrj* 4 (2017) 106–107.
- [20] F. Moreau, I. da Silva, N.H. Al Smail, T.L. Easun, M. Savage, H.G.W. Godfrey, S.F. Parker, P. Manuel, S. Yang, M. Schröder, *Nat. Commun.* 8 (2017) 14085.
- [21] R. Vaidhyanathan, S.S. Iremonger, G.K.H. Shimizu, P.G. Boyd, S. Alavi, T.K. Woo, *Science* 330 (2010) 650.
- [22] E.D. Bloch, W.L. Queen, R. Krishna, J.M. Zadrozny, C.M. Brown, *J.R. Long, Science* 335 (2012) 1606.
- [23] P. Nugent, Y. Belmabkhout, S.D. Burd, A.J. Cairns, R. Luebke, K. Forrest, T. Pham, S. Ma, B. Space, L. Wojtas, M. Eddaoudi, M.J. Zaworotko, *Nature* 495 (2013) 80–84.
- [24] Y. Peng, Y. Li, Y. Ban, H. Jin, W. Jiao, X. Liu, W. Yang, *Science* 346 (2014) 1356.
- [25] S. Yang, A.J. Ramirez-Cuesta, R. Newby, V. Garcia-Sakai, P. Manuel, S.K. Callear, S.I. Campbell, C.C. Tang, M. Schröder, *Nat. Chem.* 7 (2015) 121–129.
- [26] A. Cadiau, K. Adil, P.M. Bhatt, Y. Belmabkhout, M. Eddaoudi, *Science* 353 (2016) 137.
- [27] M.C. Das, Q. Guo, Y. He, J. Kim, C.-G. Zhao, K. Hong, S. Xiang, Z. Zhang, K.M. Thomas, R. Krishna, B. Chen, *J. Am. Chem. Soc.* 134 (2012) 8703–8710.
- [28] M.M. Wanderley, C. Wang, C.-D. Wu, W. Lin, *J. Am. Chem. Soc.* 134 (2012) 9050–9053.
- [29] Y. Inokuma, S. Yoshioka, J. Ariyoshi, T. Arai, Y. Hitora, K. Takada, S. Matsunaga, K. Rissanen, M. Fujita, *Nature* 495 (2013) 461–466.
- [30] Z. Hu, W.P. Lustig, J. Zhang, C. Zheng, H. Wang, S.J. Teat, Q. Gong, N.D. Rudd, J. Li, *J. Am. Chem. Soc.* 137 (2015) 16209–16215.

- [31] Q. Han, C. He, M. Zhao, B. Qi, J. Niu, C. Duan, *J. Am. Chem. Soc.* 135 (2013) 10186–10189.
- [32] Q.-L. Zhu, J. Li, Q. Xu, *J. Am. Chem. Soc.* 135 (2013) 10210–10213.
- [33] B. Li, K. Leng, Y. Zhang, J.J. Dynes, J. Wang, Y. Hu, D. Ma, Z. Shi, L. Zhu, D. Zhang, Y. Sun, M. Chrzanowski, S. Ma, *J. Am. Chem. Soc.* 137 (2015) 4243–4248.
- [34] H. Noh, Y. Cui, A.W. Peters, D.R. Pahls, M.A. Ortuño, N.A. Vermeulen, C.J. Cramer, L. Gagliardi, J.T. Hupp, O.K. Farha, *J. Am. Chem. Soc.* 138 (2016) 14720–14726.
- [35] Y.-T. Xu, X. Xiao, Z.-M. Ye, S. Zhao, R. Shen, C.-T. He, J.-P. Zhang, Y. Li, X.-M. Chen, *J. Am. Chem. Soc.* 139 (2017) 5285–5288.
- [36] Q. Yang, Q. Xu, H.-L. Jiang, *Chem. Soc. Rev.* 46 (2017) 4774–4808.
- [37] J.Y. An, C.M. Shade, D.A. Chengelis-Czegán, S. Petoud, N.L. Rosi, *J. Am. Chem. Soc.* 133 (2011) 1220–1223.
- [38] R.-B. Lin, F. Li, S.-Y. Liu, X.-L. Qi, J.-P. Zhang, X.-M. Chen, *Angew. Chem. Int. Ed.* 52 (2013) 13429–13433.
- [39] Y. Cui, B. Chen, G. Qian, *Coord. Chem. Rev.* 273 (2014) 76–86.
- [40] Z. Hu, B.J. Deibert, J. Li, *Chem. Soc. Rev.* 43 (2014) 5815–5840.
- [41] R.-B. Lin, S.-Y. Liu, J.-W. Ye, X.-Y. Li, J.-P. Zhang, *Adv. Sci.* 3 (2016) 1500434.
- [42] Z. Wang, K. Hu, S. Gao, H. Kobayashi, *Adv. Mater.* 22 (2010) 1526–1533.
- [43] P. Horcajada, R. Gref, T. Baati, P.K. Allan, G. Maurin, P. Couvreur, G. Férey, R.E. Morris, C. Serre, *Chem. Rev.* 112 (2012) 1232–1268.
- [44] L. Sun, C.H. Hendon, M.A. Minier, A. Walsh, M. Dincă, *J. Am. Chem. Soc.* 137 (2015) 6164–6167.
- [45] R. Xu, Y. Wang, X. Duan, K. Lu, D. Micheroni, A. Hu, W. Lin, *J. Am. Chem. Soc.* 138 (2016) 2158–2161.
- [46] X. Zhao, C. Mao, K.T. Luong, Q. Lin, Q.-G. Zhai, P. Feng, X. Bu, *Angew. Chem. Int. Ed.* 55 (2016) 2768–2772.
- [47] S. Kitagawa, R. Kitaura, S.-I. Noro, *Angew. Chem. Int. Ed.* 43 (2004) 2334–2375.
- [48] H.-C. Zhou, J.R. Long, O.M. Yaghi, *Chem. Rev.* 112 (2012) 673–674.
- [49] C. Wang, D. Liu, W. Lin, *J. Am. Chem. Soc.* 135 (2013) 13222–13234.
- [50] H.-C. Zhou, S. Kitagawa, *Chem. Soc. Rev.* 43 (2014) 5415–5418.
- [51] B. Li, M. Chrzanowski, Y. Zhang, S. Ma, *Coord. Chem. Rev.* 307 (Part 2) (2016) 106–129.
- [52] B. Li, H.-M. Wen, Y. Cui, W. Zhou, G. Qian, B. Chen, *Adv. Mater.* 28 (2016) 8819–8860.
- [53] M. Kondo, T. Yoshitomi, H. Matsuzaka, S. Kitagawa, K. Seki, *Angew. Chem. Int. Ed.* 36 (1997) 1725–1727.
- [54] W. Mori, F. Inoue, K. Yoshida, H. Nakayama, S. Takamizawa, M. Kishita, *Chem. Lett.* 26 (1997) 1219–1220.
- [55] H. Li, M. Eddaoudi, T.L. Groy, O.M. Yaghi, *J. Am. Chem. Soc.* 120 (1998) 8571–8572.
- [56] S.S.Y. Chui, S.M.F. Lo, J.P.H. Charmant, A.G. Orpen, I.D. Williams, *Science* 283 (1999) 1148.
- [57] B. Li, H. Wang, B. Chen, *Chem. Asian J.* 9 (2014) 1474–1498.
- [58] B. Li, H.-M. Wen, W. Zhou, B. Chen, *J. Phys. Chem. Lett.* 5 (2014) 3468–3479.
- [59] B. Chen, C. Liang, J. Yang, D.S. Contreras, Y.L. Clancy, E.B. Lobkovsky, O.M. Yaghi, S. Dai, *Angew. Chem. Int. Ed.* 45 (2006) 1390–1393.
- [60] P.S. Bércia, F. Zapata, J.A.C. Silva, A.E. Rodrigues, B. Chen, *J. Phys. Chem. B* 111 (2007) 6101–6103.
- [61] P.-Q. Liao, N.-Y. Huang, W.-X. Zhang, J.-P. Zhang, X.-M. Chen, *Science* 356 (2017) 1193.
- [62] Y. Wang, D. Zhao, *Cryst. Growth Des.* 17 (2017) 2291–2308.
- [63] J. Duan, W. Jin, S. Kitagawa, *Coord. Chem. Rev.* 332 (2017) 48–74.
- [64] B. Chen, S. Xiang, G. Qian, *Acc. Chem. Res.* 43 (2010) 1115–1124.
- [65] Y. Cui, B. Li, H. He, W. Zhou, B. Chen, G. Qian, *Acc. Chem. Res.* 49 (2016) 483–493.
- [66] B. Chen, S. Ma, F. Zapata, E.B. Lobkovsky, J. Yang, *Inorg. Chem.* 45 (2006) 5718–5720.
- [67] B. Chen, S. Ma, E.J. Hurtado, E.B. Lobkovsky, C. Liang, H. Zhu, S. Dai, *Inorg. Chem.* 46 (2007) 8705–8709.
- [68] B. Chen, S. Ma, E.J. Hurtado, E.B. Lobkovsky, H.-C. Zhou, *Inorg. Chem.* 46 (2007) 8490–8492.
- [69] B. Chen, S. Ma, F. Zapata, F.R. Fronczek, E.B. Lobkovsky, H.-C. Zhou, *Inorg. Chem.* 46 (2007) 1233–1236.
- [70] B. Chen, Y. Ji, M. Xue, F.R. Fronczek, E.J. Hurtado, J.U. Mondal, C. Liang, S. Dai, *Inorg. Chem.* 47 (2008) 5543–5545.
- [71] M. Xue, S. Ma, Z. Jin, R.M. Schaffino, G.-S. Zhu, E.B. Lobkovsky, S.-L. Qiu, B. Chen, *Inorg. Chem.* 47 (2008) 6825–6828.
- [72] M.C. Das, H. Xu, S. Xiang, Z. Zhang, H.D. Arman, G. Qian, B. Chen, *Chem. Eur. J.* 17 (2011) 7817–7822.
- [73] Y. He, S. Xiang, Z. Zhang, S. Xiong, F.R. Fronczek, R. Krishna, M. O’Keeffe, B. Chen, *Chem. Commun.* 48 (2012) 10856–10858.
- [74] Y. He, Z. Zhang, S. Xiang, F.R. Fronczek, R. Krishna, B. Chen, *Chem. Eur. J.* 18 (2012) 613–619.
- [75] Y. He, Z. Zhang, S. Xiang, F.R. Fronczek, R. Krishna, B. Chen, *Chem. Commun.* 48 (2012) 6493–6495.
- [76] Y. He, Z. Zhang, S. Xiang, H. Wu, F.R. Fronczek, W. Zhou, R. Krishna, M. O’Keeffe, B. Chen, *Chem. Eur. J.* 18 (2012) 1901–1904.
- [77] J. Cai, J. Yu, H. Xu, Y. He, X. Duan, Y. Cui, C. Wu, B. Chen, G. Qian, *Cryst. Growth Des.* 13 (2013) 2094–2097.
- [78] H. Xu, J. Cai, S. Xiang, Z. Zhang, C. Wu, X. Rao, Y. Cui, Y. Yang, R. Krishna, B. Chen, G. Qian, *J. Mater. Chem. A* 1 (2013) 9916–9921.
- [79] X. Duan, Y. He, Y. Cui, Y. Yang, R. Krishna, B. Chen, G. Qian, *RSC Adv.* 4 (2014) 23058–23063.
- [80] X. Duan, Q. Zhang, J. Cai, Y. Yang, Y. Cui, Y. He, C. Wu, R. Krishna, B. Chen, G. Qian, *J. Mater. Chem. A* 2 (2014) 2628–2633.
- [81] G. Chang, M. Huang, Y. Su, H. Xing, B. Su, Z. Zhang, Q. Yang, Y. Yang, Q. Ren, Z. Bao, B. Chen, *Chem. Commun.* 51 (2015) 2859–2862.
- [82] M. Huang, G. Chang, Y. Su, H. Xing, Z. Zhang, Y. Yang, Q. Ren, Z. Bao, B. Chen, *Chem. Commun.* 51 (2015) 12205–12207.
- [83] S. Xiong, Q. Liu, Q. Wang, W. Li, Y. Tang, X. Wang, S. Hu, B. Chen, *J. Mater. Chem. A* 3 (2015) 10747–10752.
- [84] O. Alduhaish, H. Wang, B. Li, T.-L. Hu, H.D. Arman, K. Alfooty, B. Chen, *ChemPlusChem* 81 (2016) 770–774.
- [85] R.A. Myers, *Handbook of Petroleum Refining Processes*, McGraw-Hill, New York, 2004.
- [86] R.V. Jasra, S.G.T. Bhat, *Sep. Sci. Technol.* 23 (1988) 945–989.
- [87] L. Alaerts, C.E.A. Kirschhock, M. Maes, M.A. van der Veen, V. Finsy, A. Depla, J.A. Martens, G.V. Baron, P.A. Jacobs, J.F.M. Denayer, D.E. De Vos, *Angew. Chem. Int. Ed.* 46 (2007) 4293–4297.
- [88] Z.-Y. Gu, D.-Q. Jiang, H.-F. Wang, X.-Y. Cui, X.-P. Yan, *J. Phys. Chem. C* 114 (2010) 311–316.
- [89] Z.-Y. Gu, X.-P. Yan, *Angew. Chem. Int. Ed.* 49 (2010) 1477–1480.
- [90] L. Pan, D.H. Olson, L.R. Ciemmolowski, R. Heddy, J. Li, *Angew. Chem. Int. Ed.* 45 (2006) 616–619.
- [91] M.P.M. Nicolau, P.S. Bércia, J.M. Gallegos, J.A.C. Silva, A.E. Rodrigues, B. Chen, *J. Phys. Chem. C* 113 (2009) 13173–13179.
- [92] Z.R. Herm, B.M. Wiers, J.A. Mason, J.M. van Baten, M.R. Hudson, P. Zajdel, C.M. Brown, N. Masciocchi, R. Krishna, J.R. Long, *Science* 340 (2013) 960.
- [93] B. Chen, X. Zhao, A. Putkham, K. Hong, E.B. Lobkovsky, E.J. Hurtado, A.J. Fletcher, K.M. Thomas, *J. Am. Chem. Soc.* 130 (2008) 6411–6423.
- [94] N.N. Greenwood, A. Earnshaw, *Chemistry of the Elements*, Elsevier Butterworth-Heinemann, Amsterdam/Heidelberg, 2005.
- [95] D. Noguchi, H. Tanaka, A. Kondo, H. Kajiro, H. Noguchi, T. Ohba, H. Kanoh, K. Kaneko, *J. Am. Chem. Soc.* 130 (2008) 6367–6372.
- [96] S.A. FitzGerald, C.J. Pierce, J.L.C. Rowsell, E.D. Bloch, J.A. Mason, *J. Am. Chem. Soc.* 135 (2013) 9458–9464.
- [97] H. Oh, M. Hirscher, *Eur. J. Inorg. Chem.* 2016 (2016) 4278–4289.
- [98] Z. Zhang, S. Xiang, B. Chen, *CrystEngComm* 13 (2011) 5983–5992.
- [99] S.-C. Xiang, Z. Zhang, C.-G. Zhao, K. Hong, X. Zhao, D.-R. Ding, M.-H. Xie, C.-D. Wu, M.C. Das, R. Gill, K.M. Thomas, B. Chen, *Nat. Commun.* 2 (2011) 204.
- [100] Y. He, R. Krishna, B. Chen, *Energy Environ. Sci.* 5 (2012) 9107–9120.
- [101] T.-L. Hu, H. Wang, B. Li, R. Krishna, H. Wu, W. Zhou, Y. Zhao, Y. Han, X. Wang, W. Zhu, Z. Yao, S. Xiang, B. Chen, *Nat. Commun.* 6 (2015) 7328.
- [102] Z. Zhang, S. Xiang, K. Hong, M.C. Das, H.D. Arman, M. Garcia, J.U. Mondal, K.M. Thomas, B. Chen, *Inorg. Chem.* 51 (2012) 4947–4953.
- [103] H.-M. Wen, B. Li, H. Wang, C. Wu, K. Alfooty, R. Krishna, B. Chen, *Chem. Commun.* 51 (2015) 5610–5613.
- [104] H.-M. Wen, B. Li, H. Wang, R. Krishna, B. Chen, *Chem. Commun.* 52 (2016) 1166–1169.
- [105] Z. Yao, Z. Zhang, L. Liu, Z. Li, W. Zhou, Y. Zhao, Y. Han, B. Chen, R. Krishna, S. Xiang, *Chem. Eur. J.* 22 (2016) 5676–5683.
- [106] R.-G. Lin, R.-B. Lin, B. Chen, *J. Solid State Chem.* 252 (2017) 138–141.
- [107] L. Zhang, X. Cui, H. Xing, Y. Yang, Y. Cui, B. Chen, G. Qian, *RSC Adv.* 7 (2017) 20795–20800.
- [108] X. Cui, K. Chen, H. Xing, Q. Yang, R. Krishna, Z. Bao, H. Wu, W. Zhou, X. Dong, Y. Han, B. Li, Q. Ren, M.J. Zaworotko, B. Chen, *Science* 353 (2016) 141–144.
- [109] R.-B. Lin, L. Li, H. Wu, H. Arman, B. Li, R.-G. Lin, W. Zhou, B. Chen, *J. Am. Chem. Soc.* 139 (2017) 8022–8028.
- [110] X. Cui, Q. Yang, L. Yang, R. Krishna, Z. Zhang, Z. Bao, H. Wu, Q. Ren, W. Zhou, B. Chen, H. Xing, *Adv. Mater.* 29 (2017) 1606929.
- [111] W. Wu, B. Han, H. Gao, Z. Liu, T. Jiang, J. Huang, *Angew. Chem. Int. Ed.* 43 (2004) 2415–2417.
- [112] P.K. Thallapally, R.K. Motkuri, C.A. Fernandez, B.P. McGrail, G.S. Behrooz, *Inorg. Chem.* 49 (2010) 4909–4915.
- [113] Z. Zhang, Z.-Z. Yao, S. Xiang, B. Chen, *Energy Environ. Sci.* 7 (2014) 2868–2899.
- [114] L. Bastin, P.S. Bércia, E.J. Hurtado, J.A.C. Silva, A.E. Rodrigues, B. Chen, *J. Phys. Chem. C* 112 (2008) 1575–1581.
- [115] S. Xiang, Y. He, Z. Zhang, H. Wu, W. Zhou, R. Krishna, B. Chen, *Nat. Commun.* 3 (2012) 954.
- [116] Z. Zhang, S. Xiang, X. Rao, Q. Zheng, F.R. Fronczek, G. Qian, B. Chen, *Chem. Commun.* 46 (2010) 7205–7207.
- [117] Y. He, S. Xiang, Z. Zhang, S. Xiong, C. Wu, W. Zhou, T. Yildirim, R. Krishna, B. Chen, *J. Mater. Chem. A* 1 (2013) 2543–2551.
- [118] H. Alawisi, B. Li, K. Alfooty, L. Wu, S. Xiang, H. Wang, B. Chen, *Inorg. Chem. Commun.* 50 (2014) 106–109.
- [119] H. Alawisi, B. Li, Y. He, H.D. Arman, A.M. Asiri, H. Wang, B. Chen, *Cryst. Growth Des.* 14 (2014) 2522–2526.
- [120] X. Duan, R. Song, J. Yu, H. Wang, Y. Cui, Y. Yang, B. Chen, G. Qian, *RSC Adv.* 4 (2014) 36419–36424.
- [121] D. Yan, B. Chen, Q. Duan, *Inorg. Chem. Commun.* 49 (2014) 34–36.
- [122] Z. Chen, S. Xiang, H.D. Arman, P. Li, S. Tidrow, D. Zhao, B. Chen, *Eur. J. Inorg. Chem.* 2010 (2010) 3745–3749.
- [123] Z. Chen, S. Xiang, H.D. Arman, P. Li, D. Zhao, B. Chen, *Eur. J. Inorg. Chem.* 2011 (2011) 2227–2231.
- [124] Z. Chen, S. Xiang, H.D. Arman, J.U. Mondal, P. Li, D. Zhao, B. Chen, *Inorg. Chem.* 50 (2011) 3442–3446.
- [125] G. Chen, Z. Zhang, S. Xiang, B. Chen, *CrystEngComm* 15 (2013) 5232–5235.

- [126] S. Xiong, Y. He, R. Krishna, B. Chen, Z. Wang, *Cryst. Growth Des.* 13 (2013) 2670–2674.
- [127] C. Song, Y. He, B. Li, Y. Ling, H. Wang, Y. Feng, R. Krishna, B. Chen, *Chem. Commun.* 50 (2014) 12105–12108.
- [128] S. Xiong, Y. Gong, H. Wang, H. Wang, Q. Liu, M. Gu, X. Wang, B. Chen, Z. Wang, *Chem. Commun.* 50 (2014) 12101–12104.
- [129] O. Alduhaish, B. Li, H. Arman, R.-B. Lin, J.C.-G. Zhao, B. Chen, *Chin. Chem. Lett.* 28 (2017) 1653–1658.
- [130] M. Xue, Z. Zhang, S. Xiang, Z. Jin, C. Liang, G.-S. Zhu, S.-L. Qiu, B. Chen, *J. Mater. Chem.* 20 (2010) 3984–3988.
- [131] Z. Zhang, S. Xiang, Y.-S. Chen, S. Ma, Y. Lee, T. Phely-Bobin, B. Chen, *Inorg. Chem.* 49 (2010) 8444–8448.
- [132] Y. He, H. Furukawa, C. Wu, M. O’Keeffe, R. Krishna, B. Chen, *Chem. Commun.* 49 (2013) 6773–6775.
- [133] Y. Yue, J.A. Rabone, H. Liu, S.M. Mahurin, M.-R. Li, H. Wang, Z. Lu, B. Chen, J. Wang, Y. Fang, S. Dai, *J. Phys. Chem. C* 119 (2015) 9442–9449.
- [134] O. Alduhaish, H. Wang, B. Li, H.D. Arman, V. Nesterov, K. Alfooty, B. Chen, *ChemPlusChem* 81 (2016) 764–769.
- [135] B. Li, B. Chen, *Sci. China Chem.* 59 (2016) 965–969.
- [136] W. Yang, G. Chang, H. Wang, T.-L. Hu, Z. Yao, K. Alfooty, S. Xiang, B. Chen, *Eur. J. Inorg. Chem.* 2016 (2016) 4470–4475.
- [137] L. Zhang, K. Jiang, M. Jiang, D. Yue, Y. Wan, H. Xing, Y. Yang, Y. Cui, B. Chen, G. Qian, *Chem. Commun.* 52 (2016) 13568–13571.
- [138] S.C. King, R.-B. Lin, H. Wang, H.D. Arman, B. Chen, *Mater. Chem. Front.* 1 (2017) 1514–1519.
- [139] H. Wang, B. Li, H. Wu, T.-L. Hu, Z. Yao, W. Zhou, S. Xiang, B. Chen, *J. Am. Chem. Soc.* 137 (2015) 9963–9970.
- [140] A. Kumar, D.G. Madden, M. Lusi, K.-J. Chen, E.A. Daniels, T. Curtin, J.J. Perry, M. J. Zaworotko, *Angew. Chem. Int. Ed.* 54 (2015) 14372–14377.
- [141] J.A. Mason, T.M. McDonald, T.-H. Bae, J.E. Bachman, K. Sumida, J.J. Dutton, S.S. Kaye, J.R. Long, *J. Am. Chem. Soc.* 137 (2015) 4787–4803.
- [142] P.M. Bhatt, Y. Belmabkhout, A. Cadiau, K. Adil, O. Shekhah, A. Shkurenko, L.J. Barbour, M. Eddaoudi, *J. Am. Chem. Soc.* 138 (2016) 9301–9307.
- [143] R. Matsuda, R. Kitaura, S. Kitagawa, Y. Kubota, R.V. Belosludov, T.C. Kobayashi, H. Sakamoto, T. Chiba, M. Takata, Y. Kawazoe, Y. Mita, *Nature* 436 (2005) 238–241.
- [144] J.-P. Zhang, X.-M. Chen, *J. Am. Chem. Soc.* 131 (2009) 5516–5521.
- [145] Z. Chen, S. Xiang, D. Zhao, B. Chen, *Cryst. Growth Des.* 9 (2009) 5293–5296.
- [146] H. Xu, Y. He, Z. Zhang, S. Xiang, J. Cai, Y. Cui, Y. Yang, G. Qian, B. Chen, *J. Mater. Chem. A* 1 (2013) 77–81.
- [147] G. Chang, B. Li, H. Wang, T. Hu, Z. Bao, B. Chen, *Chem. Commun.* 52 (2016) 3494–3496.
- [148] K.-J. Chen, H.S. Scott, D.G. Madden, T. Pham, A. Kumar, A. Bajpai, M. Lusi, K.A. Forrest, B. Space, J.J. Perry IV, M.J. Zaworotko, *Chem* 1 (2016) 753–765.
- [149] B. Li, B. Chen, *Chem* 1 (2016) 669–671.
- [150] H.-M. Wen, H. Wang, B. Li, Y. Cui, H. Wang, G. Qian, B. Chen, *Inorg. Chem.* 55 (2016) 7214–7218.
- [151] L. Zhang, C. Zou, M. Zhao, K. Jiang, R. Lin, Y. He, C.-D. Wu, Y. Cui, B. Chen, G. Qian, *Cryst. Growth Des.* 16 (2016) 7194–7197.
- [152] L. Zhang, K. Jiang, Y. Li, D. Zhao, Y. Yang, Y. Cui, B. Chen, G. Qian, *Cryst. Growth Des.* 17 (2017) 2319–2322.
- [153] P. Li, Y. He, Y. Zhao, L. Weng, H. Wang, R. Krishna, H. Wu, W. Zhou, M. O’Keeffe, Y. Han, B. Chen, *Angew. Chem. Int. Ed.* 54 (2015) 574–577.
- [154] F. Luo, C. Yan, L. Dang, R. Krishna, W. Zhou, H. Wu, X. Dong, Y. Han, T.-L. Hu, M. O’Keeffe, L. Wang, M. Luo, R.-B. Lin, B. Chen, *J. Am. Chem. Soc.* 138 (2016) 5678–5684.
- [155] L. Li, R.-B. Lin, R. Krishna, X. Wang, B. Li, H. Wu, J. Li, W. Zhou, B. Chen, *J. Am. Chem. Soc.* 139 (2017) 7733–7736.